In search of floating algae and other organisms in global oceans and lakes

Lin Qi[1,2,3], Chuanmin Hu[2*], Karlis Mikelsons[4,5], Menghua Wang[4], Veronica Lance[4,6], Shaojie Sun[1,2,3], Brian B. Barnes[2], Jun Zhao[1,3], Dimitry Van Der Zande[7]

[1]School of Marine Sciences, Sun Yat-Sen University (SYSU), Guangzhou, China

[2]College of Marine Science, University of South Florida, St. Petersburg, Florida, USA

[3]Southern Marine Science and Engineering Guangdong Laboratory (Zhuhai), Zhuhai, China

[4]National Oceanic and Atmospheric Administration, Center for Satellite Applications and Research, College Park, Maryland, USA

[5]Global Science and Technology, Inc., Greenbelt, Maryland, USA

[6]Earth System Science Interdisciplinary Center, Cooperative Institute for Satellite Earth System Studies, University of Maryland, College Park, Maryland, USA

[7]Royal Belgian Institute for Natural Sciences (RBINS), 29 Rue Vautier 29, 1000 Brussels, Belgium

*Correspondence to huc@usf.edu

Abstract

Surface floating macroalgae, microalgae, and other marine and freshwater organisms have been reported in many specific regions around the globe. However, it is technically challenging to identify similar occurrences, or other types of floating organisms or materials, within the vast global oceans and lakes. In this study, we address this challenge through combining global-scale, 375-m resolution false-colored Red-Green-Blue (FRGB) imagery from the Visible Infrared Imaging Radiometer Suite (VIIRS) in NOAA's online Ocean Color Viewer (OCView) for visual inspection and data from several other satellite sensors for spectral diagnostics. In the FRGB imagery, the near-infrared (NIR) band (862 nm) is used as the green channel, which is sensitive to floating algae and organisms/materials on the water surface. Visual inspection of the daily FRGB VIIRS imagery from January 2018 to October 2019 reveals the appearance of various slicks with different colors in many ocean regions and lakes. Combined with spectral diagnostics of the quasi-concurrent Sentinel-3A/3B Ocean and Land Colour Instrument (OLCI) and other higher spatial resolution satellite data as well as knowledge of local oceanography/limnology, most of these elongated or diffuse image features can be identified as *Ulva, Sargassum, Noctiluca, Trichodesmium, Microcystis*, oil slicks, or pumice rafts. Some of these identified features are found in regions where such occurrences have never been reported before. Some

features are of unknown type as they have not been reported previously from remote sensing. In such cases, contemporaneous scientific literature and news reports as well as spectral diagnostics allow for educated inferences to be made. One example is from surface features in the northern Gulf of Maine, Bay of Fundy, and Southwest of Nova Scotia between early June and early July of 2019. Spectral shapes of the FRGB image features indicate transparent materials lacking pigments. Knowledge of local fisheries oceanography and frequent news reports all suggest that these unknown image features may be aggregations or blooms of sea jellies and, to a lesser extent, salps. Another example is from the Great Salt Lake, where image features in the south arm of the lake are speculated to be caused by aggregations of brine shrimp eggs. Once confirmed from field sightings, these findings may represent a milestone in satellite remote sensing because previously remote sensing could only be used to infer oceanographic environments conducive to sea jellies or shrimps. In addition to the findings presented here, the approach in this study may serve as a template to discover various known and unknown types of floating algae and organisms/materials as well as to routinely monitor and track their distributions and movements.

Keywords: Remote sensing, global search, OCView, VIIRS, Sentinel-3, OLCI, Sentinel-2, MSI, Landsat-8, OLI, World-View, DOVE, floating algae, *Ulva, Sargassum, Noctiluca, Trichodesmium, Microcystis,* sea jellies, *salps,* brine shrimp, oil slicks, pumice rafts.

1. Introduction

Various types of floating algae have been reported in some of the world's oceans and lakes through satellite ocean color remote sensing. These include: cyanobacterium *Microcystis* in Lake Taihu and Lake Erie and many other lakes (Hu et al., 2010a; Wynne et al., 2010; Loftin et al., 2016), *Sargassum fluitans* and/or *natans* in the Gulf of Mexico (Gower et al., 2006) and Atlantic Ocean (Gower et al., 2013; Gower and King, 2019; Wang et al., 2019), *Ulva prolifera* in the Yellow Sea (Hu et al., 2010b; Qi et al., 2016; Xing et al., 2019), *Sargassum horneri* in the East China Sea (Qi et al., 2017), *Trichodesmium* in many ocean regions (Gower et al., 2014; McKinna et al., 2015; Blondeau-Patissier et al., 2018), red *Noctiluca scintillans* in the East China Sea (Qi et al., 2019), green *Noctiluca scintillans* in the Arabian Sea (do Rosário Gomes et al., 2014), and other aquatic plants (Dogliotti et al., 2018). Other floating materials such as oil slicks and pumice

rafts have also been reported from ocean color imagery (Hu et al., 2009; Jutzeler et al., 2014; Mantas et al., 2011).

Traditional ocean color algorithms and data products, for example, surface chlorophyll-a concentrations (Chl) (O'Reilly et al., 2000; Hu et al., 2012) and inherent optical properties (IOPs) of the water column (Lee et al., 2002; Werdell et al., 2013; Shi and Wang, 2019), cannot be used to detect and quantify these surface features in satellite imagery. One reason is because atmospheric correction algorithms that rely on the near-infrared (NIR) or shortwave infrared (SWIR) wavelengths (Gordon and Wang, 1994; Wang, 2007) often fail because of the violation of the underlying black-water assumptions due to elevated reflectance in these wavelengths by floating algae or other materials. In addition, quality control of these standard ocean color data products is often conservative, leading to data gaps in these products for at least half of the cloud-free conditions (Hu et al., 2019). To overcome these limitations, partial atmospheric correction through removal of gaseous absorption and Rayleigh scattering is often performed, following which non-traditional algorithms are used for detection and quantification. For example, floating algae index (FAI) (Hu, 2009) and alternative floating algae index (AFAI) (Qi et al., 2016; Wang and Hu, 2016) were designed to quantify the red-edge reflectance of floating algae and have been applied to study long-term changes in *Ulva* blooms in the Yellow Sea (Qi et al., 2016), *Sargassum horneri* blooms in the East China Sea (Qi et al., 2017), and *Sargassum fluitans/natans* blooms in the Atlantic (Wang et al., 2019). In such applications, customized algorithms to mask clouds, cloud shadows, straylight, and sun glint have also been developed for each study region.

One shortcoming of customized algorithms or approaches is that researchers need to develop them (for both algae detection and masking clouds and other artifacts) and then process satellite data for their regions of interest with known floating algae blooms. This is because such customized satellite data products are simply not available at a global scale. Furthermore, floating algae or other floating organisms/materials may well occur in regions not identified in previous studies, as most oceans and lakes have not been explored using these approaches. However, implementing such algorithms for global processing of satellite data at full resolution represents a daunting task for individual researchers, creating a dilemma between demand and data product availability.

In 2016, the National Oceanic and Atmospheric Administration (NOAA) of the United States implemented an online tool, Ocean Color Viewer (OCView) (Mikelsons and Wang, 2018), to visualize various ocean color data products derived from the Visible Infrared Imaging Radiometer Suite (VIIRS) on the Suomi National Polar-orbiting Partnership (SNPP) (2012–present) measurements. The data products include normalized water-leaving radiances, Chl and IOPs as well as Red-Green-Blue (RGB) true color images. All are at global scale, but with various spatial and temporal resolutions. In addition to SNPP/VIIRS, OCView also serves mission-long RGB imagery from NOAA-20 VIIRS, as well as Sentinel-3A/3B Ocean and Land Colour Instrument (OLCI), GCOM-C Second-Generation Global Imager (SGLI), and COMS Geostationary Ocean Color Imager (GOCI). Although not originally designed for detecting floating algae, the OCView tool provides an excellent framework to implement customized imagery at full resolution of the VIIRS imaging bands (i.e., 375 m), from which an approach may be developed to overcome the technical challenges inherent in detecting floating algae and other organisms/materials at global scale.

This study has the following objectives:

1. To develop an approach to detect floating algae and other floating organisms/materials at global scale;
2. To search for and document known and unknown floating algae and other organisms/materials, using spectral analysis to interpret these image features;
3. To establish a spectral dataset of known and unknown image features for future use;

We first describe the new data product implemented in OCView for the above purposes. This is followed by the description of the approach to find various floating algae features and to perform spectral analysis to identify the algae type, with findings presented in the Results section. In particular, the approach to find and interpret unknown image features is demonstrated. Finally, we discuss the significance of our findings as well as the strengths and limitations of the approach for global applications.

2. Data and Images

VIIRS SNPP FRGB data were produced at NOAA and accessed through the NOAA OCView online tool. Other remote sensing data used in this study were acquired from other sources. Further information about data and images are discussed below.

VIIRS

Although FAI and AFAI have proven useful in detecting and quantifying floating macroalgae and floating microalgae through quantifying their red-edge reflectance, some algae scums are known to be undetectable because they do not show red-edge reflectance. For example, FAI and AFAI are insensitive to surface aggregations of red *Noctiluca* because the reflectance in the 3 spectral bands used to calculate FAI or AFAI is elevated almost equally (Qi et al., 2019). These characteristics will also make the Maximum Chlorophyll Index (MCI) (Gower et al., 2005 & 2008) insensitive to detect these algal features. In addition, masking unwanted image features such as clouds, cloud shadows, sun glint, and those caused by ocean current shears while keeping the wanted features (i.e., floating algae or other organisms) is problematic at a global scale. Rather than developing and implementing algorithms to differentiate all these wanted and unwanted image features, an alternative and better approach is to implement quick-look imagery at a full resolution, so a user can make visual judgements to be supported with subsequent spectral diagnostics of these features, following the approach described here.

The quick-look imagery that has been implemented in the OCView is false-colored RGB (FRGB), where a NIR band replaced the green band from traditional RGB imagery. In this way, image features with spatial contrast from the background water pixels can be visually identified. Floating vegetation will show in a greenish color due to the enhanced NIR reflectance (i.e., the red-edge reflectance). Non-vegetative floating organisms or materials have low NIR reflectance or elevated reflectance in all three bands, which will not appear greenish but can still be visualized because they show different colors from the background water. Such FRGB imagery has been previously generated for the Moderate Resolution Imaging Spectroradiometer (MODIS) data in a Virtual Antenna System (Hu et al., 2014), from which floating macroalgae and microalgae in a marginal ocean can be visualized (Qi et al., 2019). However, FRGB at full-resolution of satellite sensors for global oceans and lakes has not been implemented in the above Virtual Antenna System or elsewhere.

The FRGB images available in the OCView tool were produced from VIIRS SNPP Level-1B data processed to Rayleigh corrected reflectance ($R_{rc}(\lambda)$, dimensionless). Then, $R_{rc}(\lambda)$ at 638 nm (375-m resolution), 862 nm (375-m resolution), and 443 nm (750-m resolution) were used to generate the FRGB images using the following stretch to convert $R_{rc}(\lambda)$ (floating point value) to $I(\lambda)$ (image byte value from 0 to 255):

$$I = 255 \times \log\left(R_{rc} \times (R_{rc}^{max} - R_{rc}^{min})/(R_{rc}^{min} \times R_{rc}^{max}) + 1\right) / \log(R_{rc}^{max} / R_{rc}^{min}), \quad (1)$$

The conversion was applied to each of the FRGB bands but for brevity the wavelength dependence is omitted here. Eq. 1 results in $I = 0$ for $R_{rc} = 0.0$ and $I = 255$ for $R_{rc} = R_{rc}^{max}$. Here R_{rc}^{min} and R_{rc}^{max} are the parameters of the conversion, determined from trial-and-error to maximize the contrast between image features and surrounding waters while keeping most of the dynamic range to visualize clouds and thick aerosols (e.g., dust). The 443-nm band was "sharpened" to 375-m resolution to match the other two bands using a scheme similar to Landsat image sharpening (Vivone et al., 2014).

OLCI

Although VIIRS has the advantage of wide swath (3,300 km) and therefore daily coverage over global oceans and lakes, it has only two spectral bands in the visible (638 nm) and NIR (862 nm) at a 375-m nominal spatial resolution, limiting the spectral diagnoses of the visually identified image features. Therefore, the VIIRS data are supplemented with data collected by OLCI on the Sentinel-3A (2016 to present) and Sentinel-3B (2018 to present) satellites for spectral diagnoses. With a swath width of 1,270 km, measurements from each OLCI cover the global ocean every two to three days. The 21 spectral bands between 400 nm and 1,020 nm, all with a nominal spatial resolution of 300 m, are particularly useful to examine the spectral shapes of the identified image feature. The full-resolution Level-1B data were downloaded from https://codarep.eumetsat.int and processed to generate $R_{rc}(\lambda)$ using the SeaDAS software package developed by NASA, which were used to compose RGB and FRGB images as well as to perform spectral analysis.

OLI, MSI, DOVE, WorldView, and Pleiades

High spatial resolution data, i.e., from the Operational Land Imager (OLI, 30 m); the Multi-Spectral Instrument (MSI, 10 and 20 m); the DOVE (3 m), WorldView (WV, 0.3 to 0.5 m panchromatic band and 1.2 m to 2 m multi-spectral bands), and Pleiades -1A from Google Earth

– 0.5 m; see Table 1), were used to complement VIIRS and OLCI in this study. For most coastal waters, these sensors have only sporadic coverage but they provide a complementary, more detailed view of the VIIRS-identified image features if they are available. The suite of satellite sensors allows for the combination of spatial detail with temporal frequency which greatly aids in identifying and tracking the features of interest.

OLI (onboard Landsat 8) data were obtained from the U.S. Geological Survey. These data cover coastal waters with a 16-day revisit frequency. MSI (onboard Sentinel-2A/2B) data were obtained from https://scihub.copernicus.eu/. The MSI sensors have more global coverage than OLI, with most regions sampled with a five-day revisit frequency when both sensors are used. DOVE data were obtained from Planet Labs, Inc (Planet Team, 2017). Designed to map the land surface, DOVE has four spectral bands in the blue, green, red, and NIR.

DigitalGlobe WV3 data were provided by the Commercial Archive Data for NASA investigators (cad4nasa.gsfc.nasa.gov) under the National Geospatial-Intelligence Agency's NextView license agreement (Neigh et al., 2013). The WV3 VNIR sensor has eight spectral bands (425.5 nm to 948 nm) and one panchromatic band (445 nm to 808 nm). Pleiades was launched by the Centre National d'Etudes Spatiales (CNES) (the Space Agency of France) in 2011, with data collected at a resolution of 0.5 m (Gaudin-Delrieu et al., 2017). Pleiades-1A images used in this study were obtained from Google Earth.

MODIS

In this study, MODIS data were used to examine spectral data corresponding to historical events when VIIRS measurements were not available. For this purpose, the use of MODIS is limited in this study. MODIS has a large swath of 2,330 km, with ~1.5 day revisit frequency of the global surface. Similar to VIIRS, MODIS has two 250-m bands at 645 and 859 nm, two 500-m bands at 469 nm and 555 nm in the visible, and seven other bands in the visible with nominal 1 km resolution. These data were downloaded from the NASA Goddard Space Flight Center.

Table 1 presents a summary of the sensor characteristics. For all these sensors, $R_{rc}(\lambda)$ data products were derived from the Level-1B radiance data using various software package: CVIIRS code from the NASA Direct Readout Laboratory for VIIRS, NASA SeaDAS for OLCI and MODIS, Acolite (Vanhellemont and Ruddick, 2015) for OLI and MSI, and computer codes

developed in house for DOVE and WV3. Then, the corresponding RGB and FRGB images were generated using the sensor-specific red, green, blue, and NIR bands. Note that of all sensors used (Table 1), only SNPP VIIRS was used to generate daily FRGB imagery, served by OCView in near real-time at the global scale. Other sensors were used to provide more detailed view (in either spectral characteristics or spatial resolution) of the image features identified in the SNPP VIIRS FRGB imagery.

3. Approach to Search for and Identify Image Features

Three steps were used in the approach, where data from VIIRS, OLCI, and higher spatial resolution sensors are all important.

First, VIIRS daily snapshot FRGB images from NOAA OCView were visually inspected. An example of the global FRGB composite of daily snapshot images is shown in Fig. 1, where various features can be visualized. In this step, clouds (whitish) and cloud shadows (dark patterns adjacent to clouds) can be easily identified. Sun glint can be easily identified because sun glint pixels form elongated shapes along the satellite track (i.e., approximately north-south). Shallow water features, small islands, or fixed offshore platforms can also be easily identified because they are static in sequential imagery. Thin clouds in FRGB imagery appear whitish and diffuse, and therefore can also be recognized. In contrast, elongated image slicks can often be found to stand out from the relatively homogenous image background. These visually identified image slicks are our study interest. Even without the subsequent spectral analyses, it is easy to understand that the image slicks with a greenish color in the FRGB imagery are due to elevated NIR reflectance of floating algae, and slicks with other colors are something else (i.e., non-vegetation organisms or materials).

Next, for the visually identified image features, the corresponding $R_{rc}(\lambda)$ data and RGB/FRGB images from concurrent (i.e., same day) and co-located OLCI, OLI, MSI, DOVE, and/or WV3 were generated. If the same-day images were not available, images from adjacent days were used. The spectral shapes of selected pixels within the image features were examined against nearby water pixels (used as references). The resulting $R_{rc}(\lambda)$ difference spectra (i.e., $R_{rc}(\lambda)$ of pixels of interest minus $R_{rc}(\lambda)$ of nearby water pixels) are named as $\Delta R_{rc}(\lambda)$, where "Δ" means difference. This "difference" technique has long been used in spectral analysis of various image features

(Gower et al., 2006 & 2019 for *Sargassum*; Qi et al., 2017 for *Ulva* and *Sargassum*; Qi et al., for red *Noctiluca*). This is because of the effect of mixed pixels, where each pixel within the features often contains a very small percentage of the floating algae or organisms/materials. Without referencing to nearby water pixels, the spectral shape of the pixel of interest is often dominated by water, and therefore cannot be distinguished from others. For example, without referencing against nearby waters it is difficult or impossible to differentiate pixels of interest as containing red *Noctiluca* surface mats (Qi et al., 2019).

Finally, information on regional oceanography, especially on dominant algae types or organisms, was obtained through literature review and online searches. This step helped to identify the type of the floating algae or organisms/materials. For example, blooms of *Ulva* macroalgae have occurred in the Yellow Sea every May – July since 2008 (Hu et al., 2010b; Qi et al., 2016; Xing et al., 2019), so greenish slicks from the FRGB images in this region in summer are highly likely to be *Ulva.* This identification could be presumed with relative confidence even without confirmation from spectral diagnostics. Such background information is particularly useful for identifying unknown image features that are difficult to determine from spectroscopy alone. In this study, we will use examples to illustrate this concept.

Visually inspecting daily FRGB imagery at 375 m resolution over the entire globe for more than a year between January 2018 and October 2019 is time consuming. Therefore, the visual inspections proceeded with two objectives: 1) Targeted searches of known floating algae blooms in selected regions, according to reports from the literature, were first conducted; 2) Exploratory searches for occurrences that were not known *a priori* were conducted in other regions.

4. Results

Results reported here demonstrate the effectiveness of this spectroscopy-based approach of diagnosing the image features and detecting known and unknown types of floating algae and organisms/materials. However, a thorough compilation of all floating algae and organisms/materials around the globe is beyond the scope of this study. We trust that others may use the same approach and available data and images for regional or global studies.

We start with Fig. 1 showing a sample daily VIIRS FRGB image composite on 9 June 2019, overlaid with approximate locations of the visually identified image features (rectangular boxes)

from other dates. Because the 862-nm band was used as the green band, land appears greenish or yellowish and water appears purplish.

Overall, 28 regions (including oceans and lakes) were found to show slick features in the FRGB imagery. After spectral diagnostics and literature review (as detailed below), most of them were found to be various types of floating algae or other organisms/materials. The identified image features are summarized in Table 2 and annotated in Fig. 1, and partitioned into four groups: Group 1 (boxes or dots with solid red lines) indicates features of known types where long-term satellite remote sensing studies are available; Group 2 (boxes or dots with dashed red lines) indicates features of known types where satellite remote sensing case studies are available; Group 3 (boxes or dots with solid blue lines) indicates features of known types where only field studies are available; Group 4 (green boxes) indicates features of unknown types based on literature review. In the summary table, due to the space limitation, the references listed are representative and not exhaustive. Below we show examples of all categories, with specific emphasis on the unknown features.

4.1. Known types of floating algae and other organisms/materials

The known floating algae examples include *Sargassum fluitans* and/or *Sargassum natans* in the Atlantic Ocean (including the Caribbean Sea and Gulf of Mexico, Box 1 in Fig. 1), *Sargassum horneri* in the East China Sea (Box 2), *Ulva prolifera* green macroalgae in the Yellow Sea (Box 3), green *Noctiluca* in the Arabian Sea (Box 7), red *Noctiluca* in the East China Sea (Boxes 8a & 8b), *Trichodesmium* in the South Pacific (including Great Barrier Reef and Fiji), South Atlantic and Eastern Bengal Bay (Boxes 4a-f), cyanobacterium *Microcystis* in Lake Erie and Lake Okeechobee in the United States, Lake Winnipeg in Canada, Lagoa dos Patos in Brazil, Lake Taihu in China and many others (Boxes 5a-e), oil slicks from natural seeps in the NW Gulf of Mexico (Box 9), and pumice rafts in the South Pacific (Box 10).

Figs. 2–7 show examples of the feature appearance in VIIRS FRGB imagery as well as their spectral shapes identified from the corresponding OLCI imagery. A brief description is provided for each of these known cases.

4.1.1. *Sargassum*

Fig. 2(a-1 and a-2) show greenish image slicks in the central tropical Atlantic due to *Sargassum fluitans* and/or *Sargassum natans*. The spectral shapes in Fig. 2(a-3) show typical red-edge

reflectance of floating vegetation, and the local reflectance maximum around 620 nm indicates brownish color of the vegetation. These image features are within the Great Atlantic *Sargassum* Belt (GASB) that occurred every summer since 2011 (except 2013) (Gower et al., 2013; Gower and King, 2019; Wang et al., 2019). Therefore, they can be inferred to be *Sargassum*, although it is impossible to distinguish spectrally whether they are *S. fluitans* or *S. natans*. Indeed, within Box 1 in Fig. 1 (tropical Atlantic, Caribbean, Gulf of Mexico), similar greenish image slicks can often be found from VIIRS FRGB images, with similar OLCI spectral shapes shown here. For example, while Fig. 2(a-1) shows an example for 28 July 2019, greenish image slicks were found in the same region in all cloud-free and glint-free FRGB images from 6 July to 15 August 2019. The pelagic *Sargassum* has been known to be abundant in the Sargasso Sea of the North Atlantic and in the Gulf of Mexico, but recent studies show the recurrent GASB. The daily 375-m resolution VIIRS FRGM imagery may provide near real-time information on the location of these ecologically important macroalgae, and such information is also useful in predicting potential *Sargassum* beaching events whereby a large amount of *Sargassum* represents a nuisance to the environment and local tourism (Hu et al., 2016).

Fig. 2(b-1 and b-2) shows greenish image slicks in the East China Sea, located in the western Pacific Ocean (Box 2 of Fig. 1). The corresponding OLCI spectra in Fig. 2(b-3) show red-edge reflectance and local reflectance maximum around 620 nm. These are typical characteristics of *Sargassum horneri* (*S. horneri*) reported in Qi et al. (2017) and Xing et al. (2017). Unlike the pelagic *Sargassum* species in the Atlantic, *S. horneri* grows on rocks, but can continue to grow after being detached from the bottom by wind storms or other perturbations. Their reflectance in the visible (Fig. 2(b-3)) is generally lower than those of the Atlantic *Sargassum* (Fig. 2(a-3)), making them appear darker to a human eye than the Atlantic *Sargassum*, likely due to their difference in pigment compositions. Nevertheless, large amounts of *S. horneri* have been reported every spring since 2012 in the East China Sea (Qi et al., 2017), calling for more studies on their ecological and environmental impacts.

4.1.2. *Ulva*

Of all macroalgae blooms, perhaps *Ulva prolifera* in the Yellow Sea (Box 3 of Fig. 1) has been studied the most, primarily due to its environmental impacts since 2008, with numerous researchers working on this phenomenon. A literature review of "Yellow Sea *Ulva*" in Google Scholar returned 10,700 results. Fig. 3a shows a VIIRS FRGB image where greenish image

334 slicks can be seen. The corresponding OLCI spectra in Fig. 3b show the red-edge reflectance as
335 well as local reflectance maximum around 560 nm, both typical for *Ulva* in this region. The *Ulva*
336 bloom in this region became well known during the 2008 Olympic sailing competition off
337 Qingdao (Hu and He, 2008; Shi and Wang, 2009), but remote sensing studies indicate that the
338 earliest bloom can be tracked back to 2007 (Hu et al., 2010b), and a clear trend of increased
339 bloom size every May – July in recent years is evident (Qi et al., 2016; Hu et al., 2017; Xiao et
340 al., 2019; Xing et al., 2019). The recurrent blooms have been shown to be a result of coastal
341 mariculture of *Porphyra yezoensis* (commonly known as nori seaweed) (Hu et al., 2010b; Liu et
342 al., 2009; Xing et al., 2019). With the blooms being projected to be recurrent in future years, the
343 daily VIIRS FRGB imagery can be used to help monitor and track these blooms.

344 #### 4.1.3. *Noctiluca scintillans*

345 *Noctiluca scintillans* is a marine dinoflagellate that feeds on other marine phytoplankton and
346 small microzooplankton. When disturbed, they can produce bioluminescence, and at high
347 concentrations they can form red tides. Two forms of *Noctiluca*, green *Noctiluca* and red
348 *Noctiluca*, are found in all temperate, subtropical, and tropical coastal waters (Elbrächter and Qi,
349 1998, Harrison et al., 2011). *Green Noctiluca* blooms in the Arabian Sea have been studied with
350 satellite remote sensing (do Rosário Gomes et al., 2008; 2014). However, differentiating green
351 *Noctiluca* blooms from other blooms often requires diagnostic information in addition to remote
352 sensing spectroscopy (Thibodeau et al., 2014). At high concentrations, however, they can form
353 surface scums which display red-edge reflectance characteristics observable in FRGB imagery.
354 In contrast, because of the unique absorption and spectral shapes (Van Mol et al., 2007), red
355 *Noctiluca* blooms can be differentiated from other blooms even from remote sensing
356 spectroscopy alone (Qi et al., 2019).

357 Figs. 4(a-1) and 4(b-1) show two examples of a red *Noctiluca* bloom and a green *Noctiluca*
358 bloom in the East China Sea and Arabian Sea, respectively. Similar to those reported in Qi et al.
359 (2019), red *Noctiluca* image slicks appear greyish (Fig. 4(a-1) and 4(a-2)) but green *Noctiluca*
360 image slicks appear greenish (Fig. 4(b-1) and 4(b-2)) in the FRGB imagery. Their spectral
361 shapes in these examples (Figs. 4(a-3) and 4(b-3)) show the expected sharp increases from ~ 500
362 nm to ~600 nm for the former but a local reflectance maximum around 560 nm for the latter.
363 These spectral characteristics may be used to find red *Noctiluca* and green *Noctiluca* blooms in
364 regions without any previous reports. For example, a red *Noctiluca* bloom was captured in VIIRS

FRGB imagery over coastal waters of the Tasmania (Southern Australia) on 18 November 2018 (B8d in Table 2) for which no other report could be found from either refereed or gray literature.

4.1.4. *Trichodesmium*

Trichodesmium is a cyanobacteria that can fix (assimilate) dissolved nitrogen, resulting in a significant source of "new" nitrogen into otherwise oligotrophic oceans (Capone et al., 1997). Previous remote sensing efforts studying *Trichodesmium* have relied on absorptions of their unusual pigments of phycourobilin, phycoerythrobilin, and phycocyanin (Hu et al., 2010c; Subramaniam et al., 1999; Westberry and Siegel, 2006) and red-edge reflectance when high concentrations of *Trichodesmium* form surface scums (Subramanium et al., 2001; Hu et al., 2010c; Gower et al., 2014; see review by McKinna, 2015).

Fig. 5 shows several examples of image slicks that appear greenish in the VIIRS FRGB images that are believed to be caused by *Trichodesmium* aggregations or blooms. These examples cover waters around the Great Barrier Reefs (GBR) (Fig. 5(a-1)), Fiji Island (Fig. 5(b-1)), eastern Madagascar (Fig. 5(c-1)), and southeast Brazil (Fig. 5(d-1)), respectively. For brevity, the case for the north Gulf of California (B4-g in Table 2 and Fig. 1) is not discussed here. The reflectance spectral shapes of these image features show those of typical *Trichodesmium* blooms on the surface, with red-edge reflectance and local reflectance maximum around 560 nm – 620 nm. While some *Trichodesmium* blooms such as those around the GBR have been reported repeatedly (Blondeau-Patissier et al., 2018), others have only been reported in individual case studies (Furnas 1992; Revelante et al., 1982). The most comprehensive study by Blondeau-Patissier et al. (2018) used satellite observations to document the long-term patterns of the GBR *Trichodesmium* blooms, but they showed blooms only in waters west of 153°E. The example in Fig. 5(a-1) shows *Trichodesmium* slicks that extend farther east of 153°E. *Trichodesmium* slicks are actually found from VIIRS FRGB imagery in nearly all coastal waters around Australia, some of which have never been reported (e.g., coastal waters off SW Australia near Perth, coastal waters south of West Papua, Indonesia). Whether these unreported slicks were previously overlooked or new expansions in recent years deserves further investigation. Likewise, changes in *Trichodesmium* blooms over the past 20 years in other regions need more research, particularly using time-series analyses of satellite data (e.g., Gower et al., 2014; Blondeau-Patissier et al., 2018).

4.1.5. *Microcystis*

Microcystis aeruginosa, often called blue-green algae, is a kind of bloom-forming cyanobacteria distributed around the world. *Microcystis* blooms have been reported in many freshwater lakes and brackish waters, due mainly to eutrophication (Paerl and Huisman 2008). Of these, Lake Taihu (China) (Hu et al., 2010a; Wang et al., 2011) and Lake Erie (US) (Wynne et al., 2010) are two of the most studied lakes due to their annual bloom occurrence and impacts on drinking water, fisheries, environment, and local economy. Under calm weather, *Microcystis* can form surface scums, making them visible in FRGB imagery. Fig. 6 show examples of VIIRS FRGB images over several lakes and Lagoa dos Patos (SE Brazil), respectively, where the features that appear to be greenish in the FRGB images are due to *Microcystis* surface scums. Their spectral shapes clearly indicate the red-edge reflectance as well as the local reflectance maximum around 560 nm, which are characteristics of *Microcystis* scums. Although FAI, AFAI, and other red-edge based indices, e.g., MCI (Gower et al., 2005 & 2008), Cyanobacteria Index (CI) (Wynne et al., 2010), are adequate to quantify the bloom intensity and long-term changes (Hu et al., 2010a; Qi et al., 2018; Wynne et al., 2010), the VIIRS FRGB imagery provides a quick and easy way to visualize and monitor the blooms with daily updates, thus facilitating coordinated field efforts to measure and characterize the blooms. This is particularly important for lakes with similar blooms but with far fewer studies, for example Lake Winnipeg (Canada) (Fig. 6(a-1)) and Lake Okeechobee (US) (Fig. 6(b-1)). For Lake Winnipeg, several studies have used remote sensing to characterize the long-term changes of water quality, including the use of MERIS MCI to show bloom intensity and extent (Binding et al., 2018). Because MERIS stopped functioning in 2012 but VIIRS has been in orbit since 2011, VIIRS data may be used to fill the recent gaps in documenting bloom patterns once blooms are identified from the FRGB imagery. For Lake Okeechobee, although some studies have used remote sensing to document long-term changes of water quality (e.g., turbidity, Wang et al., 2012), similar studies of *Microcystis* blooms cannot be found in the literature, despite numerous news reports on bloom occurrence in recent years. The capacity of VIIRS FRGB imagery in tracking blooms both retrospectively and in near real-time can therefore complement existing field-based efforts in monitoring the lake's water quality.

The case of Lagoa dos Patos (Fig. 6(c-1)) is different from others, as very few studies reported *Microcystis* blooms in this subtropical, shallow lagoon (Lobo et al., 2009). The spectral shapes in Fig. 6(c-3) and the diffuse spatial patterns in Fig. 6(c-1) all indicate that these image features are

caused by aggregations of cyanobacteria. *Microcystis* blooms have additionally been identified in VIIRS FRGB imagery in many other lakes (e.g., Lake Chaohu in China, Lake Van in Turkey). For brevity, these cannot be all presented here but interested readers can inspect the online imagery through OCView and read the relevant literature for more information.

4.1.6. *Oil slicks and pumice rafts*

Oil has different optical properties (refraction index, absorption, scattering) from water; therefore it can be detected from ocean color imagery through its contrast from nearby water (Sun and Hu, 2019). In particular, because oil can suppress surface capillary waves and change surface roughness, even thin oil sheens can be observed from ocean color imagery as long as some degree of sun glint is present (Adamo et al., 2009; Hu et al., 2009; Sun and Hu, 2016). Figs. 7(a-b) show two examples of surface oil slicks in the NW Gulf of Mexico captured in VIIRS FRGB images. These oil slicks are known to originate from natural oil seeps, and they can be either darker (Fig. 7a) or brighter (Fig. 7b) than the surrounding water, depending on the sun glint strength (Hu et al., 2009; Jackson and Alpers, 2010; Lu et al., 2016). Although it is still technically challenging to estimate oil slick thickness, spectral analyses using all visible, NIR, and SWIR bands have shown potential toward differentiating various oil types (sheen, crude oil, or oil emulsion) (Clark et al., 2010; Sun and Hu, 2019; Lu et al., 2019). The VIIRS FRGB imagery provide a rapid means to identify slick features in regions that are prone to oil spills from either natural seeps or human activities (e.g., Persian Gulf, southern Caribbean, Caspian Sea), from which more in-depth analysis using other sensors and/or field measurements may be initiated.

Similar to oil seeps that seep oil from the ocean floor, silicic volcanic eruptions from the ocean floor can result in mobile accumulations of low-density pumice clasts, called pumice rafts. These pumice rafts are believed to be a nutrient source to favor algae growth (e.g., *Trichodesmium*) (Jutzeler et al., 2014; Mantas et al., 2011). In the past, satellite imagery has been used to track pumice rafts and study their fates (Jutzeler et al., 2014; Mantas et al., 2011), but overall remote sensing studies of pumice rafts are limited. Here, VIIRS FRGB images in early August 2019 show pumice rafts in the south Pacific (Fig. 7(c-1)), where these rafts show greyish colors in the FRGB images, with the corresponding OLCI spectral shapes (Fig. 7(c-2)) being different from all other floating algae or oil slicks.

In summary, while the examples presented here are by no means complete, they demonstrate the capacity of the proposed approach of combining online VIIRS FRGB imagery and other satellite data in revealing features caused by many known floating algae blooms and floating materials. Furthermore, in some regions, the areal extent of the detected bloom is beyond any previous studies, and in some other regions the blooms have not been studied through remote sensing. As such, these findings call for more in-depth studies incorporating remote sensing to understand long-term changes of bloom patterns.

4.2. Unknown types of floating features

While the capacity of this approach in detecting and classifying floating algae blooms, oil slicks, or pumice rafts has been demonstrated above, another valuable role for the approach is to search for and discover unknown image features, and then attempt to spectrally identify the features. Below we show several examples representing new findings. In two such examples, the feature types might be inferred from remote sensing spectroscopy, comparison with known spectra of various materials, media reports, and knowledge of local oceanography and fisheries. In several other examples, the feature types simply cannot be identified, therefore require further investigations.

4.2.1. Surface features in waters of north Gulf of Maine, Bay of Fundy, and off Nova Scotia: blooms of sea jellies?

Between 8 June 2019 and 3 July 2019, various slicks have been identified from waters of north Gulf of Maine, Bay of Fundy, and southwest of Nova Scotia. Figs. 8–10 show some examples from VIIRS, MSI, DOVE, Pleiades, and WV3 where the surface slicks can be seen clearly at different locations, dates, and spatial resolutions. Furthermore, Fig. 8c and Fig. 9 inset show the ΔR_{rc} spectra of several selected pixels from the OLCI and WV3 observations, respectively.

Although these slicks appear bright, clouds or foams (whitecaps) can be easily ruled out because 1) multiple images from VIIRS, OLCI, and MODIS on the same day several hours apart show that these features are almost static in time, and 2) wind speed (obtained from the National Center for Environmental Prediction) is very low, often < 3 m s^{-1} at most of the slick locations. Furthermore, reflectance of whitecaps are higher in wavelengths of 400 – 555 nm than in the NIR wavelengths (Frouin et al., 1996; Moore et al., 2000), but reflectance of these slick features are higher in the NIR wavelengths than in wavelengths of 400 – 555 nm (Fig. 8c from OLCI and Fig. 9 inset from WV3). Therefore, the slicks must be caused by organisms/materials on the

water surface. Different from the known types of floating macroalgae and microalgae, these features do not appear greenish in VIIRS and OLCI FRGB imagery, indicating lack of red-edge reflectance, and therefore they must be some non-vegetative organisms or other non-living materials. Indeed, $\Delta R_{rc}(\lambda)$ spectral shapes of the pixels of these features from sensors of various spatial resolutions and spectral bands all indicate lack of pigment absorption and rather smooth spectra where reflectance increases from the blue to the green and red wavelengths. Thus, the question is what floating organisms or materials could lead to such spectral shapes?

In an effort to differentiate *Sargassum* from other floating algae and materials, Hu et al. (2015) showed typical reflectance spectral shapes of several man-made floating materials, including white polyfoam, grey Styrofoam, and transparent plastic bottles, whose reflectance spectra are shown in Fig. 8d. These spectra were measured from such experimental, man-made "garbage" in Tampa Bay (Florida, USA), after which the items were collected from Tampa Bay and disposed. Although the spectral shapes of our Tampa Bay observations are similar to those shown in Fig. 8c & Fig. 9 insets, this much area of garbage in these coastal waters is unlikely without accompanying public media coverage, which we did not find. Alternatively, however, when transparent marine organisms such as stinging sea jellies and non-stinging moon jellies (*Cnidaria*), non-stinging comb jellies (*Ctenophora*) or salps (*subphylum Tunicata* of the *Chordata phylum*) aggregate at the surface they may appear similar to what is shown in Fig. 8c & Fig. 9 insets. Such commonly found marine organisms in these waters include *Salpa aspera* (salps), *Cyanea capillata* (sea jellies), and *Pelagia noctiluca* (sea jellies) (Laurence Madin, personal comm.). Indeed, laboratory measured reflectance spectra of several types of sea jellies found in Belgian coastal waters (der Zande et al., 2014), especially *Chrysaora hysoscella* (Fig. 8d right y-axis), do resemble those of transparent plastic bottles and image pixels from the unknown surface features because they all show spectrally smooth reflectance due to the lack of pigment absorption (der Zande et al., 2014).

Therefore, from the perspective of remote sensing spectroscopy, the slick features could be caused by blooms of "transparent" sea jellies or salps. Although laboratory measured reflectance of salps is not available, they are expected to have similar reflectance spectral shapes as those of sea jellies and plastic bottles. However, several arguments may be made to infer that these features are more likely sea jellies rather than salps.

First, salps rarely aggregate at the surface except at night (Laurence Madin, personal comm.). Second, the 0.5-m resolution Pleiades-1A (Google Earth) image on 10 June 2019 (Fig. 10a) shows round-shaped features, although the details of these features are smeared. Third, an online video posted to social media shows a surface bloom of sea jellies north of Nova Scotia in July 2019 (Fig. 10b, photo credit: Leslie Carter). Although the time and location of this reported bloom does not correspond exactly to the features in Fig. 8, similar events were reported in waters around Nova Scotia in the same month. Fourth, online reports did indicate that surface blooms of sea jellies can be of scales measurable by satellites (Nickell et al., 2010). An example is shown in Fig. 10c (image posted online on 9 June 2019), where a bloom of sea jellies occurred in Milne Bay Province, Papua New Guinea. Lastly, due to climate change (increased temperature and decreased dissolved oxygen), sea jellies blooms are believed to have increased in recent years (Condon et al., 2013; Condon et al., 2011; Mills 2001; Nickell et al., 2010).

Therefore, considering all supporting arguments above, we speculate that the unknown features observed in Figs. 8–10 are due to blooms of sea jellies. However, this inference cannot completely rule out the possibility that they are due to blooms of salps, as salps can form long chains of several meters and they have also been caught on beaches or waters near beaches in the study region.

In any case, if the inference of sea jellies is true, these features might be expected to reappear in this region in similar months (June–July) of future years, thus calling for targeted field surveys to confirm these speculations and to study what oceanographic conditions favor these blooms.

4.2.2. Surface features in the Great Salt Lake: brine shrimp cysts or algae slicks?

With a surface area of about 4,000 km^2, the Great Salt Lake is the largest salt lake in the western hemisphere. Although often called the "America's Dead Sea," the Great Salt Lake is home to native birds, brine shrimp, shorebirds, waterfowl, and several types of algae. Separated by a west-east railroad causeway, the north and south arms are different in their salinity and biota. The south arm is dominated mainly by green algae or blue-green algae (i.e., cyanobacteria) while the north arm is dominated by *Dunaliella salina* and *haloarchaea*, giving the water an unusual reddish color.

Fig. 11a shows a VIIRS FRGB image over the Great Salt Lake on 9 June 2019, where image slicks can be found in both arms of the lake. For the north arm, OLCI $\Delta R_{rc}(\lambda)$ in Fig. 11b show

spectral shapes different from all those shown above, with slight increases from the blue wavelengths to the red wavelengths but then a decrease in the NIR wavelengths. For the south arm, OLCI $\Delta R_{rc}(\lambda)$ in Fig. 11c also show different spectral shapes from the above: a sharp increase from 560 nm to 709 nm, and then a plateau in the NIR wavelengths.

A literature review indicates that in addition to algae, the Great Salt Lake is rich in brine shrimp (Belovsky et al., 2011; Jensen, 1918; Wurtsbaugh and Gliwicz, 2001), where resting shrimp eggs (cysts) can aggregate on the surface, forming reddish slicks in digital photos and high-resolution Google Earth and MSI images (Fig. 12). Furthermore, studies conducted by the Utah Division of Wildlife Resources indicate that although brine shrimp can be found occasionally in the north arm, most brine shrimp are found in the south arm (https://wildlife.utah.gov/gsl/index.php). Therefore, we speculate that the image features with spectral shapes of Fig. 11c are possibly due to surface aggregations of brine shrimp eggs under calm conditions. The spectral shapes observed (Fig. 11c) show the increase of reflectance starts from 560 nm with a lack of pigment absorption feature around 670 nm. This pattern is possibly a signature reflectance of brine shrimp cysts, yet to be confirmed by future field and/or laboratory measurements. Wind speed on 9 June 2019 was only 0 – 2 m s^{-1}, facilitating surface aggregations of shrimp eggs. Indeed, similar image slicks have been found from VIIRS FRGB imagery over another salt-water lake (the South Aral Sea, B16 in Table 2 and Fig. 1), whose spectral shapes are nearly identical to those in Fig. 11c. Brine shrimps have been found in the Aral Sea since 1998 (Arashkevich et al., 2009), further strengthening the inference that the image features in the southern Great Salt Lake are due to brine shrimp eggs. In contrast, for pixels with spectral shapes of Fig. 11b, based on literature review and without additional information, we simply cannot interpret them here. As prior remote sensing investigations of this lake have focused on general water quality (Crosman and Horel, 2009; Hansen et al., 2017), the findings here call for more field measurements of spectral reflectance specifically targeted to these features.

4.2.3. Other unknown features

Many slick features in the VIIRS FRGB imagery are not spectrally differentiated. Several examples of such features are presented in Fig. 13. These features have spectral characteristics similar to those of *Sargassum* and *Trichodesmium* as they all show local reflectance maximum around 620 nm (Figs. 13(a-2) & (b-2)). However, *Sargassum* or *Trichodesmium* blooms

occurring in fresh waters of Lake Albert (Fig. 13(a-1)) and Lake Victoria (Fig. 13(b-1)) are unlikely to our knowledge and based on literature review. Some field studies reported cyanobacterial blooms in Lake Victoria (Haande et al., 2011; Kimambo et al., 2019; Miles et al., 2013), but the reported blooms were always in nearshore waters (e.g., Murchison Bay, Nyanza Gulf) as opposed to offshore waters in Fig. 13(b-1). It is suspected that the greenish image features in Lake Albert and Lake Victoria are possibly caused by some types of freshwater brown algae, yet lack of local reports (from either remote sensing or field measurements) prevents making any conclusions here. This remotely-sensed identification of these offshore features could justify executing and precisely guide field studies farther offshore in these lakes.

Likewise, Fig. 13(c-1) shows some greenish slicks in the VIIRS FRGB image over the northern Persian (Arabian) Gulf. Because green *Noctiluca* blooms often occur in this region, one may speculate that these image slicks are caused by a green *Noctiluca* bloom. However, the corresponding OLCI spectra do not show local reflectance maximum around 560 nm, but instead show local reflectance maximum around 620 nm, with a slight decrease at 560 nm. These are characteristics of *Trichodesmium*. Yet a literature review returned no report of *Trichodesmium* blooms in this region. Because these image features are recurrent, the only possible way to resolve the puzzles of differentiating these unknown features is through targeted field surveys in the future.

5. Discussion

5.1. Detecting floating algae and other organisms/materials at global scale

Blooms of floating macroalgae (e.g., *Ulva*, *Sargassum*) and certain types of microalgae (e.g., *Microcystis, Noctiluca*, *Trichodesmium*) have been reported in several regions of global oceans and lakes from field studies and satellite remote sensing. In a few cases, long-term bloom trends have also been reported, but in many other cases it is unclear whether the remotely sensed floating algae blooms are episodic events, annually recurrent, or have experienced temporal changes or trends in the past 20 years. Similarly, the global spatial extent of regionally reported floating algae blooms is not well known, and it is unclear whether currently undocumented and unknown types of floating algae and floating organisms/materials also occur in some regions of the global oceans and lakes. Due to lack of medium-resolution, customized remote sensing data products at the global scale, these questions have been difficult to address in the past.

607 Addressing such questions now shows great promise through the approach demonstrated here,
608 which is to combine visual inspection of the global medium-resolution VIIRS FRGB imagery in
609 OCView with spectral analysis of OLCI and other higher-spatial resolution remote sensing data.
610 Previously, a similar approach was used by Gower et al. (2008) to examine the MCI anomalies
611 from 1.2-km resolution MERIS data at the global scale, yet MCI is insensitive to some of the
612 features identified here (e.g., red *Noctiluca*, pumice, oil slicks, the unknown floating features in
613 the north arm of the Great Salt Lake). The approach here uses finer spatial resolution (375-m)
614 and wider-swath VIIRS FRGB imagery at the global-scale with daily updates to improve
615 coverage and sensitivity. Additionally, visual inspection of such imagery, often in conjunction
616 with VIIRS RGB for the identical scene, can avoid typical false positive detection due to thin
617 clouds, cloud shadows, thick aerosols, and other confounding factors and at the same time avoid
618 false negative detection of certain known and unknown features (e.g., red *Noctiluca*, "sea jellies"
619 features) as compared with other popular indexes such as FAI, AFAI, or MCI. The visual
620 inspection, although labor intensive, is possible at the global scale with the 375-m resolution
621 FRGB imagery and, more importantly, leaves the judgement of various confounding factors to
622 the user's visual inspection, so subsequent spectral analysis can be performed to classify feature
623 types.

624 Although one could imagine future machine learning approaches when many more observations
625 are identified, currently our approach exploiting the visual inspection of the VIIRS FRGB and
626 spectral and spatial analysis of other sensors is critical in obtaining the following two new
627 findings in this study. First, some of the known types of floating algae (*Trichodesmium*, red
628 *Noctiluca*) have been found in regions that have never been reported before. These include
629 *Trichodesmium* to the east of the Great Barrier Reefs and south of Australia, both recurrent in
630 2018 and 2019, and red *Noctiluca* in coastal waters of Tasmania, Vietnam, and Japan. Are they
631 due to expansion of the previously reported blooms? The finding provides a framework to
632 initialize targeted studies to examine the history of the unreported occurrence of floating algae in
633 these regions.

634 Second, image features of two unknown types have been discovered and inferred to be
635 aggregations of sea jellies in the northwest Atlantic and brine shrimp eggs in the Great Salt Lake.
636 For the case of the NW Atlantic sea jellies, the image features have never been reported in any
637 previous study to our knowledge. Although no concurrent ship sightings existed or were found to

638 confirm this inference, such an inference is to our knowledge the most reasonable interpretation.
639 Although these features are relatively ephemeral in the same locations, the same features did last
640 for several weeks in adjacent locations, thus future sightings from satellite imagery in the same
641 months of June–July may be used to trigger cruise surveys of these marine organisms. For the
642 case of the images speculated to be brine shrimp eggs in the Great Salt Lake, this finding may
643 open the pathway to study brine shrimp ecology and dynamics as well as their long-term changes
644 in response to climate variability and human activities. The similarity of the spectral shapes of
645 the image slicks to those from another salt lake (the South Aral Sea), which is known to have
646 aggregations of brine shrimp eggs, also supports the hypothesis that the image features in the
647 southern arm of the Great Salt Lake are due to brine shrimp eggs. In both cases, once confirmed
648 from field surveys, the discovery of these organisms may represent a new milestone in using
649 satellite remove sensing to directly detect these marine and lake organisms themselves in
650 addition to making observations of oceanic and atmospheric environments.

651 One may argue that even without the approach shown here, one could still use OLCI, MODIS,
652 MSI, OLI, or other sensors to obtain the same findings above. This might appear feasible,
653 especially with the availability of fine-resolution global quick-look OLI and MSI imagery from
654 the USGS Explorer or Copernicus or other online tools (e.g., https://s3view.oceandatalab.com/;
655 https://apps.sentinel-hub.com/sentinel-playground/) that may provide a better capacity for the
656 same "search and discover" purpose. However, OLI is restricted to coastal waters only, and the
657 high-resolution of MSI (10 m in some bands) actually makes it very difficult or even impossible
658 for visual inspection of the global oceans and lakes unless the approximate time and location are
659 known *a priori*. Indeed, without the proposed approach and especially without the availability of
660 global VIIRS FRGB imagery at 375-m resolution, it is almost impossible to know where and
661 when to search for the image features (especially those unknown features reported here) in the
662 first place, as one cannot visually inspect the entire high-resolution online imagery (MSI, OLI)
663 over global oceans and lakes for 1-2 years, and FRGB images from OLCI or MODIS at medium
664 resolution are not currently available at the global scale.

665 There is no reason to believe that the findings presented here (Fig. 1 and Table 2) are complete
666 for *all* known and unknown types of floating algae and other organisms/materials in global
667 oceans and lakes. Indeed, we encourage others to take the same approach to discover more
668 features in their regions of interest, leading to possibly more new findings. Similarly, the

669 approach is useful for regional oceanography, as local researchers can always inspect the online
670 FRGB images for their region of interest for at least two purposes: 1) use the identified features
671 to guide field sampling effort and 2) conduct retrospective analysis using other satellite data to
672 examine historical patterns of these features. The approach and the findings here are therefore
673 expected to promote research on floating algae and on other floating organisms/materials (e.g.,
674 oil slicks and pumice rafts) at the global scale.

675 *5.2. Limitations of the VIIRS FRGB imagery in OCView*

676 The global VIIRS FRGB imagery as displayed in OCView play a central role in the approach to
677 search for and classify known and unknown types of floating algae and other
678 organisms/materials. Perhaps the most difficult task in a study like this is knowing where and
679 when to search for floating algae which have rarely or never been reported. The global FRGB
680 imagery at 375-m resolution provides an optimal compromise between coverage and resolution
681 for this purpose. On the other hand, the global FRGB image set is also limited in several aspects.
682 For example, they only provide initial quick-look information, where more in-depth analysis on
683 the spectral characteristics of the identified image features may require other products or even
684 data from other satellites (e.g., OLCI spectral data) as well as analytical skills and knowledge of
685 local oceanography from the user end. Furthermore, for the same reasons that allow relatively
686 fast inspection of the VIIRS medium-resolution imagery at global scale, these images are not
687 able to detect small-scale features (e.g., several hundred meters in size) that may be well
688 detectable in OLI and MSI imagery. Likewise, the advantage of using FRGB to visually
689 differentiate realistic ocean surface features (due to floating algae or other organisms/materials)
690 from other unwanted image features comes at the price of losing some sensitivity in feature
691 detection. For comparison, some weak image features in the AFAI or MCI imagery may not
692 show up in the corresponding FRGB imagery even though the color stretch of the latter has been
693 optimized through Eq. 1. For this reason, some floating algae may be more difficult to visualize
694 than others. For example, on average, *Sargassum* mats in the East China Sea appeared to be eight
695 times less dense than *Ulva* mats in the Yellow Sea (Qi et al., 2017), making the visual detection
696 of *Sargassum* more difficult than the visual detection of *Ulva* in VIIRS FRGB imagery. However,
697 Fig. 2 and many other FRGB images in the East China Sea and the Atlantic Ocean (including the
698 Caribbean Sea and Gulf of Mexico) clearly revealed greenish image slicks due to *Sargassum*
699 *horneri* in the former and *Sargassum fluitans/natans* in the latter, even though some small or less

dense *Sargassum* rafts may be missed. Nevertheless, given the inherent spatial resolution of the VIIRS global FRGB imagery, additional effort with this approach will likely yield many additions to the list of floating algae occurrences shown in Fig. 1 and Table 2 and, overall, the global applications of this approach may be regarded as a success.

Finally, the spectral analysis of various image features identified in this study resulted in a spectral dataset to serve as a reference for future studies. The dataset is mostly based on OLCI measurements for several reasons: 1) OLCI data have medium resolution (300-m) for all spectral bands, therefore avoiding spectral distortion when combining spectral bands of different resolutions from the same sensor (e.g., 250-m, 500-m, and 1000-m resolution of MODIS; 375-m and 750-m of VIIRS, 10-m and 20-m of MSI); 2) OLCI has more spectral bands in the visible and NIR than any other existing ocean color sensors; 3) Each OLCI has at least 2-3 day revisit frequency (higher in high-latitude regions), enabling spectral diagnostics of VIIRS-identified features; and 4) OLCI data are available from Copernicus/EUMETSAT at no cost to researchers. The spectral shapes shown in the various examples above represent typical spectra from the features identified in this study. Although their magnitudes depend on the sub-pixel proportion of the algae/organism coverage, their spectral shapes are more stable, and therefore can serve as references for future studies requiring spectral diagnostics. On the other hand, OLCI is still limited in its number of spectral bands, and most of the identifications of the image features are based not only on the OLCI spectral data but also on knowledge of local oceanography/limnology as well as on the published literature and/or news reports. This is because different types of floating algae (e.g., *Ulva* versus green *Noctiluca* or cyanobacteria) are spectrally similar in these multi-band spectra. From the perspective of remote sensing spectroscopy, it is desirable to collect hyperspectral reflectance data from all these known and unknown features from either field measurements or remote sensing, from which an improved spectral library may be established for global applications. For example, the chlorophyll-c absorption feature around 625 nm for *Sargassum* can be well differentiated from hyperspectral data (Dierssen et al., 2015; Hu et al., 2015). The U.S. NASA's PACE mission (Plankton, Aerosol, Cloud, ocean Ecosystem), to be started in 2022, will hopefully provide unprecedented hyperspectral data at global scale to fill this data gap.

6. Conclusion

We demonstrate an approach to search for and identify various types of floating algae and organisms/materials in global oceans and lakes. The approach combines a recent addition in the NOAA OCView tool, namely FRGB imagery at 375-m resolution for the entire globe with daily updates, and spectral data from OLCI and other higher-resolution sensors for the purpose of search and classification. Once surface floating features in the VIIRS FRGB imagery are visually identified, more in-depth spectral analysis from other satellite data together with knowledge of local oceanography or limnology can differentiate the feature type, from which time-series studies using historical satellite data may be initiated in the future. At least two significant findings are obtained from applications of the approach over global oceans and lakes: some of the known floating algae (e.g., *Trichodesmium*, red *Noctiluca*) are found to appear in previously unreported regions, and some unknown image features are discovered and inferred to be aggregations of sea jellies and brine shrimp eggs. Other unknown features are also identified, calling for targeted local research. These results, in addition to the near real-time availability of VIIRS FRGB images global wide, compel the same approach by local communities to search for more known and unknown types of floating algae and organisms/materials, from which more in-depth analysis may be initiated to study their historical occurrences and dynamics.

Acknowledgements

This work was supported by the National Natural Science Foundation of China (No. 41806208) (Qi), the U.S. NOAA (U.S. NOAA, NA15OAR4320064) (Hu), and the U.S. NASA (NNX14AL98G, NNX16AR74G, NNX17AE57G) (Hu). We thank NASA, NOAA, USGS, and Planet Labs, Inc. and Google Earth for providing satellite data. We also thank Prof. Laurence Madin (Woods Hole Oceanographic Institution) for the insightful discussions on sea jellies and salps. DigitalGlobe data were provided by the Commercial Archive Data for NASA investigators (cad4nasa.gsfc.nasa.gov) under the National Geospatial-Intelligence Agency's NextView license agreement. The views, opinions, and findings contained in this paper are those of the authors and should not be construed as an official NOAA or U.S. Government position, policy, or decision. Three anonymous reviewers provided extensive comments to help improve the presentation of this work, whose efforts are appreciated.

References

[1] Adamo, M., De Carolis, G., De Pasquale, V., & Pasquariello, G. (2009). Detection and tracking of oil slicks on sun-glittered visible and near infrared satellite imagery. *International Journal of Remote Sensing, 30*, 6403-6427.

[2] Arashkevich, E.G., Sapozhnikov, P.V., Soloviov, K.A., Kudyshkin, T.V., & Zavialov, P.O. (2009). Artemia parthenogenetica (Branchiopoda: Anostraca) from the Large Aral Sea: Abundance, distribution, population structure and cyst production. *Journal of Marine Systems, 76*, 359-366.

[3] Belovsky, G.E., Stephens, D., Perschon, C., Birdsey, P., Paul, D., Naftz, D., Baskin, R., Larson, C., Mellison, C., & Luft, J.J.E. (2011). The Great Salt Lake Ecosystem (Utah, USA): long term data and a structural equation approach, 2, 1-40.

[4] Binding, C.E., Greenberg, T.A., McCullough, G., Watson, S.B., & Page, E. (2018). An analysis of satellite-derived chlorophyll and algal bloom indices on Lake Winnipeg. *Journal of Great Lakes Research, 44*, 436-446.

[5] Blondeau-Patissier, D., Brando, V.E., Lønborg, C., Leahy, S.M., & Dekker, A.G. (2018). Phenology of Trichodesmium spp. blooms in the Great Barrier Reef lagoon, Australia, from the ESA-MERIS 10-year mission. PloS one, 13, e0208010. https://doi.org/10.1371/journal.pone.0208010 .

[6] Capone, D.G., Zehr, J.P., Paerl, H.W., Bergman, B., & Carpenter, E.J. (1997). Trichodesmium, a Globally Significant Marine Cyanobacterium. *Science, 276*(5316), 1221-1229.

[7] Clark, R.N., Swayze, G.A., Leifer, I., Livo, K.E., Kokaly, R., Hoefen, T., Lundeen, S., Eastwood, M., Green, R.O., Pearson, N., Sarture, C., McCubbin, I., Roberts, D., Bradley, E., Steele, D., Ryan, T., Dominguez, R., and the Airborne Visible/Infrared Imaging Spectrometer (AVIRIS) Team (2010), A method for quantitative mapping of thick oil spills using imaging spectroscopy: U.S. Geological Survey Open-File Report 2010-1167, 51 p. http://pubs.usgs.gov/of/2010/1167/.

[8] Condon, R.H., Duarte, C.M., Pitt, K.A., Robinson, K.L., Lucas, C.H., Sutherland, K.R., Mianzan, H.W., Bogeberg, M., Purcell, J.E., & Decker, M.B. (2013). Recurrent jellyfish blooms are a consequence of global oscillations. *Proceedings of the National Academy of Sciences, 110*, 1000-1005.

[9] Condon, R.H., Steinberg, D.K., Del Giorgio, P.A., Bouvier, T.C., Bronk, D.A., Graham, W.M., & Ducklow, H.W. (2011). Jellyfish blooms result in a major microbial respiratory sink of carbon in marine systems. *Proceedings of the National Academy of Sciences, 108*, 10225-10230.

[10] Crosman, E.T., & Horel, J.D. (2009). MODIS-derived surface temperature of the Great Salt Lake. *Remote Sensing of Environment, 113*, 73-81.

[11] Dierssen, H. M., Chlus, A., and Russell, B. (2015). Hyperspectral discrimination of floating mats of seagrass wrack and the macroalgae Sargassum in coastal waters of Greater Florida Bay using airborne remote sensing. *Remote Sensing of Environment*, *167,* 247-258.

[12] Dogliotti, A. L., Gossn, J. I., Vanhellemont, Q., and Ruddick, K. G. (2018). Detecting and Quantifying a Massive Invasion of Floating Aquatic Plants in the Río de la Plata Turbid Waters Using High Spatial Resolution Ocean Color Imagery. *Remote Sensing*, 10(7), 1140. https://doi.org/10.3390/rs10071140.

[13] do Rosário Gomes, H., Goes, J.I., Matondkar, S.G.P., Buskey, E.J., Basu, S., Parab, S., & Thoppil, P. (2014). Massive outbreaks of Noctiluca scintillans blooms in the Arabian Sea due to spread of hypoxia. *Nature communications*, 5, 4862. 10.1038/ncomms5862.

[14] do Rosário Gomes, H., Goes, J.I., Matondkar, S.P., Parab, S.G., Al-Azri, A.R., & Thoppil, P.G. (2008). Blooms of Noctiluca miliaris in the Arabian Sea—An in situ and satellite study. *Deep Sea Research Part I: Oceanographic Research Papers, 55*, 751-765.

[15] Elbrächter, M., & Qi, Z. (1998). Aspects of Noctiluca (Dinophyceae) population dynamics. *Physiological ecology of harmful algal blooms* (pp. 315-335). Berlin: Springer.

[16] Frouin, R., Schwindling, M., & Deschamps, P.Y. (1996). Spectral reflectance of sea foam in the visible and near-infrared: In situ measurements and remote sensing implications. *Journal of Geophysical Research: Oceans, 101*, 14361-14371.
[17] Furnas, M. (1992). Pelagic Trichodesmium (= Oscillatoria) in the Great Barrier Reef region. *Marine Pelagic Cyanobacteria: Trichodesmium and other Diazotrophs* (pp. 265-272): Springer.
[18] Gaudin-Delrieu, C., Lamard, J.-L., Cheroutre, P., Bailly, B., Dhuicq, P., & Puig, O. (2017). The high resolution optical instruments for the Pleiades HR Earth observation satellites. In, *International Conference on Space Optics 2008*. Toulouse, France: SPIE.
[19] Gordon, H.R., & Wang, M. (1994). Retrieval of water-leaving radiance and aerosol optical thickness over the oceans with SeaWiFS: a preliminary algorithm. *Applied optics, 33*, 443-452.
[20] Gower, J., Hu, C., Borstad, G., King, S. (2006). Ocean color satellites show extensive lines of floating Sargassum in the Gulf of Mexico. *IEEE Transactions on Geoscience and Remote Sensing*, 44, 3619-3625.
[21] Gower, J., & King, S. (2019) The distribution of pelagic Sargassum observed with OLCI. *International Journal of Remote Sensing*, 1-11. doi:10.1080/01431161.2019.1658240.
[22] Gower, J., King, S., Borstad, G., & Brown, L. (2005). Detection of intense plankton blooms using the 709 nm band of the MERIS imaging spectrometer. *International Journal of Remote Sensing, 26*, 2005-2012.
[23] Gower, J., King, S., & Goncalves, P. (2008). Global monitoring of plankton blooms using MERIS MCI. *International Journal of Remote Sensing*, 29, 6209-6216.
[24] Gower, J., King, S., & Young, E. (2014). Global remote sensing of Trichodesmium. *International Journal of Remote Sensing, 35*, 5459-5466.
[25] Gower, J., Young, E., and King, S. (2013). Satellite images suggest a new *Sargassum* source region in 2011. *Remote Sensing Letters*, 4, 764-773.
[26] Haande, S., Rohrlack, T., Semyalo, R.P., Brettum, P., Edvardsen, B., Lyche-Solheim, A., Sørensen, K., & Larsson, P. (2011). Phytoplankton dynamics and cyanobacterial dominance in Murchison Bay of Lake Victoria (Uganda) in relation to environmental conditions. *Limnologica-Ecology Management of Inland Waters, 41*, 20-29.
[27] Hansen, C., Burian, S., Dennison, P., & Williams, G. (2017). Spatiotemporal variability of lake water quality in the context of remote sensing models. *Remote Sensing, 9* (5), 409. https://doi.org/10.3390/rs9050409.
[28] Hansson, M., & Hakansson, B. (2007). The Baltic Algae Watch System-a remote sensing application for monitoring cyanobacterial blooms in the Baltic Sea. *Journal of Applied Remote Sensing*, 1, 011507. https://doi.org/10.1117/1.2834769.
[29] Harrison, P.J., Furuya, K., Glibert, P.M., Xu, J., Liu, H., Yin, K., Lee, J.H., Anderson, D.M., Gowen, R., Al-Azri, A.J.C.J.o.O., & Limnology (2011). Geographical distribution of red and green Noctiluca scintillans. *Chinese Journal of Oceanology and Limnology, 29*, 807-831.
[30] Havens, K.E., Hanlon, C., & James, R.T. (1994). Seasonal and spatial variation in algal bloom frequencies in Lake Okeechobee, Florida, USA. *Lake Reservoir Management, 10*, 139-148.
[31] Hu, C. (2009). A novel ocean color index to detect floating algae in the global oceans. *Remote Sensing of Environment, 113*, 2118-2129.
[32] Hu, C., Barnes, B. B., Feng, L., Wang, M. & Jiang, L. (2019). On the interplay between ocean color data quality and data quantity: Impacts of quality control flags. *IEEE Geoscience and Remote Sensing Letters*, doi:10.1109/LGRS.2019.2936220.
[33] Hu, C., Barnes, B.B., Murch, B., & Carlson, P. (2014). Satellite-based virtual buoy system to monitor coastal water quality. *Optical Engineering, 53*, 051402-051402.
[34] Hu, C., Cannizzaro, J., Carder, K.L., Muller-Karger, F.E., & Hardy, R. (2010c). Remote detection of Trichodesmium blooms in optically complex coastal waters: Examples with MODIS full-spectral data. *Remote Sensing of Environment, 114*, 2048-2058.
[35] Hu, C., Feng, L., Hardy, R.F., & Hochberg, E.J. (2015). Spectral and spatial requirements of remote measurements of pelagic Sargassum macroalgae. *Remote Sensing of Environment, 167*, 229-246.

[36] Hu, C., & He, M.X. (2008). Origin and offshore extent of floating algae in Olympic sailing area. *Eos, 89*, 302-303.
[37] Hu, C., Lee, Z., & Franz, B. (2012). Chlorophyll a algorithms for oligotrophic oceans: A novel approach based on three-band reflectance difference. *Journal of Geophysical Research: Oceans (1978–2012), 117*, C01011. https://doi.org/10.1029/2011JC007395.
[38] Hu, C., Lee, Z., Ma, R., Yu, K., Li, D., & Shang, S. (2010a). Moderate resolution imaging spectroradiometer (MODIS) observations of cyanobacteria blooms in Taihu Lake, China. *Journal of Geophysical Research: Oceans (1978–2012), 115*, C04002. https://doi.org/10.1029/2009JC005511.
[39] Hu, C., Li, D., Chen, C., Ge, J., Muller-Karger, F.E., Liu, J., Yu, F., & He, M.X. (2010b). On the recurrent Ulva prolifera blooms in the Yellow Sea and East China Sea. *Journal of Geophysical Research: Oceans (1978–2012), 115*, C05017. https://doi.org/10.1029/2009JC005561
[40] Hu, C., Li, X., Pichel, W.G., & Muller-Karger, F.E. (2009). Detection of natural oil slicks in the NW Gulf of Mexico using MODIS imagery. *Geophysical Research Letters, 36*, L01604. https://doi.org/10.1029/2008GL036119.
[41] Hu, C., Murch, B., Barnes, B.B., Wang, M., Maréchal, J.-P., Franks, J., Johnson, D., Lapointe, B., Goodwin, D., & Schell, J. (2016). Sargassum watch warns of incoming seaweed. *Eos, 97*, 10-15.
[42] Hu, L., Hu, C., & Ming-Xia, H. (2017). Remote estimation of biomass of Ulva prolifera macroalgae in the Yellow Sea. *Remote Sensing of Environment, 192*, 217-227.
[43] IOCCG (2014). IOCCG (2014). Phytoplankton Functional Types from Space. Sathyendranath, S. (ed.), Reports of the International Ocean-Colour Coordinating Group, No. 15, IOCCG, Dartmouth, Canada.
[44] Jackson, C. R., and W. Alpers (2010), The role of the critical angle in brightness reversals on sunglint images of the sea surface, J. Geophys. Res., 115(C9), doi:10.1029/2009jc006037.
[45] Jensen, A.C. (1918). Some observations on Artemia gracilis, the brine shrimp of Great Salt Lake. *The Biological Bulletin, 34*, 18-32.
[46] Jutzeler, M., Marsh, R., Carey, R.J., White, J.D.L., Talling, P.J., & Karlstrom, L. (2014). On the fate of pumice rafts formed during the 2012 Havre submarine eruption. *Nature communications, 5*, 3660. 10.1038/ncomms4660 | www.nature.com/naturecommunications.
[47] Jyothibabu, R., Madhu, N., Murukesh, N., Haridas, P., Nair, K., & Venugopal, P. (2003). Intense blooms of Trichodesmium erythraeum (Cyanophyta) in the open waters along east coast of India. *Indian Journal of Marine Sciences, 32*, 165-167.
[48] Kimambo, O.N., Gumbo, J.R., & Chikoore, H. (2019). The occurrence of cyanobacteria blooms in freshwater ecosystems and their link with hydro-meteorological and environmental variations in Tanzania. *Heliyon, 5*, e01312. https://doi.org/10.1016/j.heliyon.2019.e01312.
[49] Lam, N., & Hai, D. (1996). Harmful marine phytoplankton in Vietnam waters. In T. Yasumoto, Y. O'shima, & Y. Fukuyo (Eds.), Harmful toxic algal blooms. Athens, Greece.
[50] Lee, Z., Carder, K.L., & Arnone, R.A. (2002). Deriving inherent optical properties from water color: a multiband quasi-analytical algorithm for optically deep waters. *Applied optics, 41*, 5755-5772.
[51] Liu, D., Keesing, J.K., Xing, Q., & Shi, P. (2009). World's largest macroalgal bloom caused by expansion of seaweed aquaculture in China. *Marine Pollution Bulletin, 58*, 888-895.
[52] Lobo, F.d.L., Barbosa, C.C.F., Novo, E.M.L.d.M., & Yunes, J.S. (2009). Mapping potential cyanobacterial bloom using Hyperion/EO-1 data in the Patos Lagoon estuary. *Acta Limnol. Bras, 21*, 299-308.
[53] Loftin, K.A., Graham, J.L., Hilborn, E.D., Lehmann, S.C., Meyer, M.T., Dietze, J.E., & Griffith, C.B. (2016). Cyanotoxins in inland lakes of the United States: Occurrence and potential recreational health risks in the EPA National Lakes Assessment 2007. *Harmful Algae, 56*, 77-90.
[54] Lu, Y., Shi, J., Wen, Y., Hu, C., Zhou, Y., Sun, S., Zhang, M., Mao, Z., & Liu, Y. (2019). Optical interpretation of oil emulsions in the ocean – Part I: Laboratory measurements and proof-of-concept with AVIRIS observations. *Remote Sensing of Environment, 230*, 111183. https://doi.org/10.1016/j.rse.2019.05.002.

908 [55] Lu, Y., Sun, S., Zhang, M., Murch, B., & Hu, C. (2016). Refinement of the critical angle calculation
909 for the contrast reversal of oil slicks under sunglint. *Journal of Geophysical Research: Oceans, 121*,
910 148-161.
911 [56] Mantas, V.M., Pereira, A.J.S.C., & Morais, P.V. (2011). Plumes of discolored water of volcanic
912 origin and possible implications for algal communities. The case of the Home Reef eruption of 2006
913 (Tonga, Southwest Pacific Ocean). *Remote Sensing of Environment, 115*, 1341-1352.
914 [57] McKinna, L.I.W. (2015). Three decades of ocean-color remote-sensing Trichodesmium spp. in the
915 World's oceans: A review. *Progress in Oceanography, 131*, 177-199.
916 [58] McLeod, D.J., Hallegraeff, G.M., Hosie, G.W., & Richardson, A.J. (2012). Climate-driven range
917 expansion of the red-tide dinoflagellate *Noctiluca scintillans* into the Southern Ocean. *Journal of*
918 *Plankton Research, 34*, 332-337.
919 [59] Belovsky, G. E., D. Stephens, C. Perschon, P. Birdsey, D. Paul, D. Naftz, R. Baskin, C. Larson, C.
920 Mellison, J. Luft, R. Mosley, H. Mahon, J. Van Leeuwen, and D. V. Allen. 2011. The Great Salt
921 Lake Ecosystem (Utah, USA): long term data and a structural equation approach. *Ecosphere*
922 2(3):art33. doi:10.1890/ES10-00091.1.
923 [60] Mikelsons, M., & Wang, M. (2018). Interactive online maps make satellite ocean data accessible.
924 *Eos, 99,* doi:10.1029/2018EO096563.
925 [61] Miles, C.O., Sandvik, M., Nonga, H.E., Rundberget, T., Wilkins, A.L., Rise, F., & Ballot, A. (2013).
926 Identification of microcystins in a Lake Victoria cyanobacterial bloom using LC–MS with thiol
927 derivatization. *Toxicon, 70*, 21-31.
928 [62] Mills, C.E. (2001). Jellyfish blooms: are populations increasing globally in response to changing
929 ocean conditions? *Hydrobiologia, 451*, 55-68.
930 [63] Moore, K. D., Voss, K. J., and Gordon, H. R. (2000). Spectral reflectance of whitecaps: Their
931 contribution to water-leaving radiance, *Journal of Geophysical Research*. 105, 6493–6499.
932 [64] Neigh, C.S., Masek, J.G., & Nickeson, J.E. (2013). High-resolution satellite data open for
933 government research. *Eos, 94 (13)*, 121-123.
934 [65] Nickell, T., Davidson, K., Fox, C., Miller, P., and Hays, G. (2010). Developing the capacity to
935 monitor the spatial and temporal distribution of jellyfish in western Scottish waters. *The Crown*
936 *Estate*, 70 pages. ISBN: 978-1-906410-23-0.
937 [66] O'Reilly, J. E., et al. (2000), SeaWiFS postlaunch calibration and validation analyses, Part 3, NASA
938 Tech. Memo., NASA, TM-2000-206892, vol. 11,49 pp.
939 [67] Paerl, H.W., & Huisman, J. (2008). Blooms Like It Hot. *Science, 320*, 57-58.
940 [68] Planet Team (2017). Planet Application Program Interface. In: Space for Life on Earth. San
941 Francisco, CA. https://api.planet.com.
942 [69] Post, A., Dedej, Z., Gottlieb, R., Li, H., Thomas, D., El-Absawi, M., El-Naggar, A., El-Gharabawi,
943 M., & Sommer, U. (2002). Spatial and temporal distribution of Trichodesmium spp. in the stratified
944 Gulf of Aqaba, Red Sea. *Marine Ecology Progress Series, 239*, 241-250.
945 [70] Qi, L., Hu, C., Visser, P.M., & Ma, R. (2018). Diurnal changes of cyanobacteria blooms in Taihu
946 Lake as derived from GOCI observations. *Limnology and Oceanography, 63*, 1711-1726.
947 [71] Qi, L., Hu, C., Wang, M., Shang, S., & Wilson, C. (2017). Floating Algae Blooms in the East China
948 Sea. *Geophysical Research Letters, 44*, 11,501-511,509.
949 [72] Qi, L., Hu, C., Xing, Q., & Shang, S. (2016). Long-term trend of Ulva prolifera blooms in the
950 western Yellow Sea. *Harmful Algae, 58*, 35-44.
951 [73] Qi, L., Tsai, S.-F., Chen, Y., Le, C., & Hu, C. (2019). In Search of Red Noctiluca scintillans Blooms
952 in the East China Sea,*Geophysical Research Letters*, 46, 5997-6004.
953 [74] Revelante, N., Williams, W., & Bunt, J. (1982). Temporal and spatial distribution of diatoms,
954 dinoflagellates and Trichodesmium in waters of the Great Barrier Reef. *Journal of Experimental*
955 *Marine Biology Ecology, 63*, 27-45.
956 [75] Shi, W. and Wang, M. (2009). Green macroalgae blooms in the Yellow Sea during the spring and
957 summer of 2008. *J. Geophys. Res.*, 114, C12010, http://dx.doi.org/10.1029/2009JC005513.

[76] Shi, W., & Wang, M. (2019). A blended inherent optical property algorithm for global satellite ocean color observations. *Limnology and Oceanography: Methods, 17*, 377-394.
[77] Subramaniam, A., Brown, C.W., Hood, R.R., Carpenter, E.J., & Capone, D.G. (2001). Detecting Trichodesmium blooms in SeaWiFS imagery. *Deep Sea Research Part II: Topical Studies in Oceanography, 49*, 107-121.
[78] Subramaniam, A., Carpenter, E.J., & Falkowski, P.G. (1999). Bio-optical properties of the marine diazotrophic cyanobacteria Trichodesmium spp. II. A reflectance model for remote sensing. *Limnology and Oceanography:, 44*, 618-627.
[79] Sun, S., & Hu, C. (2016). Sun glint requirement for the remote detection of surface oil films. *Geophysical Research Letters, 43*, 309-316.
[80] Sun, S., & Hu, C. (2019). The Challenges of Interpreting Oil–Water Spatial and Spectral Contrasts for the Estimation of Oil Thickness: Examples From Satellite and Airborne Measurements of the Deepwater Horizon Oil Spill. *IEEE Transactions on Geoscience Remote Sensing, 57*, 2643-2658.
[81] Tada, K., Pithakpol, S., & Montani, S. (2004). Seasonal variation in the abundance of Noctiluca scintillans in the Seto Inland Sea, Japan. *Plankton Biology and Ecology, 51*, 7-14.
[82] Thibodeau, P.S., Roesler, C.S., Drapeau, S.L., Prabhu Matondkar, S., Goes, J.I., & Werdell, P.J. (2014). Locating Noctiluca miliaris in the Arabian Sea: An optical proxy approach. *Limnology and Oceanography, 59*, 2042-2056.
[83] V. der Zande, D., Green, J., & Ruddick, K. (2014). JellySpec: feasibility study for determining the spectral characteristics of jellyfish from Belgian waters. In, *Ocean Optics XXII*, Portland, USA, 26 – 31 October, 2014, 7pp.
[84] Van Mol, B., Ruddick, K., Astoreca, R., Park, Y., & Nechad, B. (2007). Optical detection of a Noctiluca scintillans bloom. *EARSeL eProceedings, 6*, 130-137.
[85] Vanhellemont, Q., & Ruddick, K. (2015). Advantages of high quality SWIR bands for ocean colour processing: Examples from Landsat-8. *Remote Sensing of Environment, 161*, 89-106.
[86] Vivone, G., Alparone, L., Chanussot, J., Mura, M.D., Garzelli, A., Member, S., Licciardi, G.A., Restaino, R., & Wald, L. (2014). Pansharpening Algorithms. *IEEE Trans. Geosci. Remote Sens. 53*, 2565–2586.
[87] Wang, M. (2007). Remote sensing of the ocean contributions from ultraviolet to near-infrared using the shortwave infrared bands: simulations. *Applied optics, 46*, 1535-1547.
[88] Wang, M., & Hu, C. (2016). Mapping and quantifying Sargassum distribution and coverage in the Central West Atlantic using MODIS observations. *Remote Sensing of Environment, 183*, 350-367.
[89] Wang, M., Hu, C., Barnes, B.B., Mitchum, G., Lapointe, B., & Montoya, J.P. (2019). The great Atlantic Sargassum belt. *Science, 365*, 83-87.
[90] Wang, M., Nim, C.J., Son, S., & Shi, W. (2012). Characterization of turbidity in Florida's Lake Okeechobee and Caloosahatchee and St. Lucie estuaries using MODIS-Aqua measurements. *Water Research, 46*, 5410-5422.
[91] Wang, M., Shi, W., and Tang, J. (2011). Water property monitoring and assessment for China's inland Lake Taihu from MODIS-Aqua measurements. *Remote Sensing of Environment*, 115, 841–845.
[92] Werdell, P.J., Franz, B.A., Bailey, S.W., Feldman, G.C., Boss, E., Brando, V.E., Dowell, M., Hirata, T., Lavender, S.J., & Lee, Z. (2013). Generalized ocean color inversion model for retrieving marine inherent optical properties. *Applied optics, 52*, 2019-2037.
[93] Westberry, T.K., & Siegel, D.A. (2006). Spatial and temporal distribution of *Trichodesmium* blooms in the world's oceans. *Global Biogeochemical Cycles, 20*, GB4016. https://doi.org/10.1029/2005GB002673.
[94] White, A. E., Prahl, F. G., Letelier, R. M., and Popp, B. N. (2007), Summer surface waters in the Gulf of California: Prime habitat for biological N_2 fixation, *Global Biogeochem. Cycles*, 21, GB2017, doi:10.1029/2006GB002779.

[95] White, A.E., Foster, R.A., Benitez-Nelson, C.R., Masqué, P., Verdeny, E., Popp, B.N., Arthur, K.E., & Prahl, F.G. (2013). Nitrogen fixation in the Gulf of California and the Eastern Tropical North Pacific. *Progress in Oceanography, 109*, 1-17.
[96] Wurtsbaugh, W.A., & Gliwicz, Z.M. (2001). Limnological control of brine shrimp population dynamics and cyst production in the Great Salt Lake, Utah. *Saline Lakes* (pp. 119-132): Springer.
[97] Wynne, T.T., Stumpf, R.P., Tomlinson, M.C., & Dyble, J. (2010). Characterizing a cyanobacterial bloom in western Lake Erie using satellite imagery and meteorological data. *Limnology and Oceanography, 55*, 2025-2036.
[98] Xiao, Y., Zhang, J., Cui, T., Gong, J., Liu, R., Chen, X., & Liang, X. (2019). Remote sensing estimation of the biomass of floating Ulva prolifera and analysis of the main factors driving the interannual variability of the biomass in the Yellow Sea. *Marine Pollution Bulletin, 140*, 330-340.
[99] Xing, Q., An, D., Zheng, X., Wei, Z., Wang, X., Li, L., Tian, L., & Chen, J. (2019). Monitoring seaweed aquaculture in the Yellow Sea with multiple sensors for managing the disaster of macroalgal blooms. *Remote Sensing of Environment, 231*, 111279. https://doi.org/10.1016/j.rse.2019.111279.
[100] Xing, Q., Guo, R., Wu, L., An, D., Cong, M., Qin, S., & Li, X. (2017). High-Resolution Satellite Observations of a New Hazard of Golden Tides Caused by Floating Sargassum in Winter in the Yellow Sea. *IEEE Geoscience and Remote Sensing Letters, 14*, 1815-1819.

Table 1. Satellite sensors used in this study, together with their characteristics in spectral and spatial resolutions and revisit frequency. Note: although all sensors collected data for many years, only some of them were used in this study to achieve the specific objectives. *These bands do not include the thermal bands. Note that in this study, only VIIRS imagery are obtained from the NOAA OCView, while data from all other sensors are obtained elsewhere.

Sensor	Bands* (nm)	Res. (m)	Revisit	Duration	Source
VIIRS	15; 415 – 2250	375, 750	Daily	2012 –	NOAA
MODIS	20; 412 – 2130	250, 500, 1000	1-2 days	2000 –	NASA
OLCI	21; 400 – 1020	300	2-3 days	2016 –	Copernicus
OLI	9; 440 – 2200	30	16 days	2013 –	USGS
MSI	12; 443 – 2190	10, 20, 60	5 days	2015 –	Copernicus
DOVE	4; 475 – 785	3 – 5	Irregular	2013 –	Planet
Pleiades	4; 430 – 950	0.5 – 2	4 – 26 days	2011 –	Google Earth
WV3	8; 400 – 1040	0.31 – 3.7	Irregular	2014 –	NASA

Table 2. Descriptions of image features shown in numbered boxes in Fig. 1. Some of these are illustrated below using VIIRS FRGB and other satellite images together with spectral diagnostics. See text for more details. Note that the images on these specific dates are meant to give examples of the findings, and similar images can be found in adjacent days and in 2018. The references are also meant to examples instead of being exhaustive. RS: remote sensing.

Box #		Location	Image Date	FRGB-Color	Type	References	Comments
B1		Atlantic Ocean	07/28/2019	Green	*S. fluitans or S. natans* (Marco algae)	Wang et al. (2019)	Long-term RS studies
B2		East China Sea	04/18/2019	Green	*S. horneri* (Marco algae)	Qi et al. (2017)	Long-term RS studies
B3		Yellow Sea	06/23/2019	Green	*Ulva prolifera* (Marco algae)	Qi et al. (2016)	Long-term RS studies
B4	4a	South Atlantic (Brazil)	01/30/2019	Green	*Trichodesmium* (Cyanobacterium)	Subramaniam et al. (2001)	RS case studies
	4b	Red Sea	5/12/2019			Post et al. (2002)	RS case studies
	4c	Madagascar	11/24/2018			Gower et al. (2014)	Field studies
	4d	Western Bay of Bengal	02/22/2019			Jyothibabu et al. (2003)	Field studies
	4e	Australia	03/18/2019			Blondeau-Patissier et al. (2018)	Long-term RS studies
	4f	Fiji (South Pacific)	11/24/2018			IOCCG report (2014)	RS case studies
	4-g	N Gulf of California	10/23/2019			White et al. (2013)	Field studies
B5	5a	Lake Winnipeg (Canada)	08/01/2019	Green	*Microcystis* (Cyanobacterium)	Binding et al. (2018)	Long-term RS studies
	5b	Lake Erie (U. S.)	07/10/2019			Wynne et al. (2010)	Long-term RS studies

B5	5c	Lake Okeechobee (U. S.)	06/21/2019	Green	*Microcystis* (Cyanobacterium)	Havens et al. (1994)	Field studies
	5d	Lagoa dos Patos (Brazil)	02/28/2019			Lobo et al. (2009)	RS case studies
	5e	Lake Taihu (China)	05/22/2019			Hu et al. (2010)	Long-term RS studies
B6		Baltic Sea-Gulf of Finland	07/20/2019	Green	*Nodularia, Anabaena, Microcystis* (Cyanobacteria)	Hansson and Hakansson (2007)	Long-term RS studies
B7		Arabian Sea	03/14/2019	Green	Green *Noctiluca* (Dinoflagellate)	Gomes et al. (2014)	Long-term RS studies
B8	8a	East China Sea	06/08/2019	Brown	Red *Noctiluca* (Dinoflagellate)	Qi et al. (2017)	Long-term RS studies
	8b	Japan	05/05/2017			Tada et al. (2004)	Field studies
	8c	Vietnam	02/15/2019			Lam and Hai (1996)	Field studies
	8d	Tasmania (Australia)	11/18/2018			McLeod et al. (2012)	Field studies
B9		NW Gulf of Mexico	05/17/2019	Dark	Oil slicks	Hu et al. (2009)	RS case studies
			07/19/2019	Bright			
B10		South Pacific	08/11/2019	Gray	Pumice rafts	Jutzeler et al. (2014)	RS case studies
B11		Nova Scotia- Gulf of Maine	06/09/2019	Gray	Sea jellies?	Online and media reports	
B12		Great Salt Lake (U. S.)	06/09/2019	Green	Brine shrimp eggs?	Online and media reports	
			06/09/2019	White	Unknown feature	No report	
B13		Lake Albert (East Africa)	08/11/2019	Green	Unknown algae	No report	
B14		Lake Victoria (East Africa)	07/20/2019	Green	Unknown algae	No report	
B15		North Persian Gulf	05/15/2019	Green	Unknown algae	No report	

B16	Aral Sea (Central Asia)	10/19/2019	Green	Brine shrimp eggs?	Arashkevich et al. (2009)

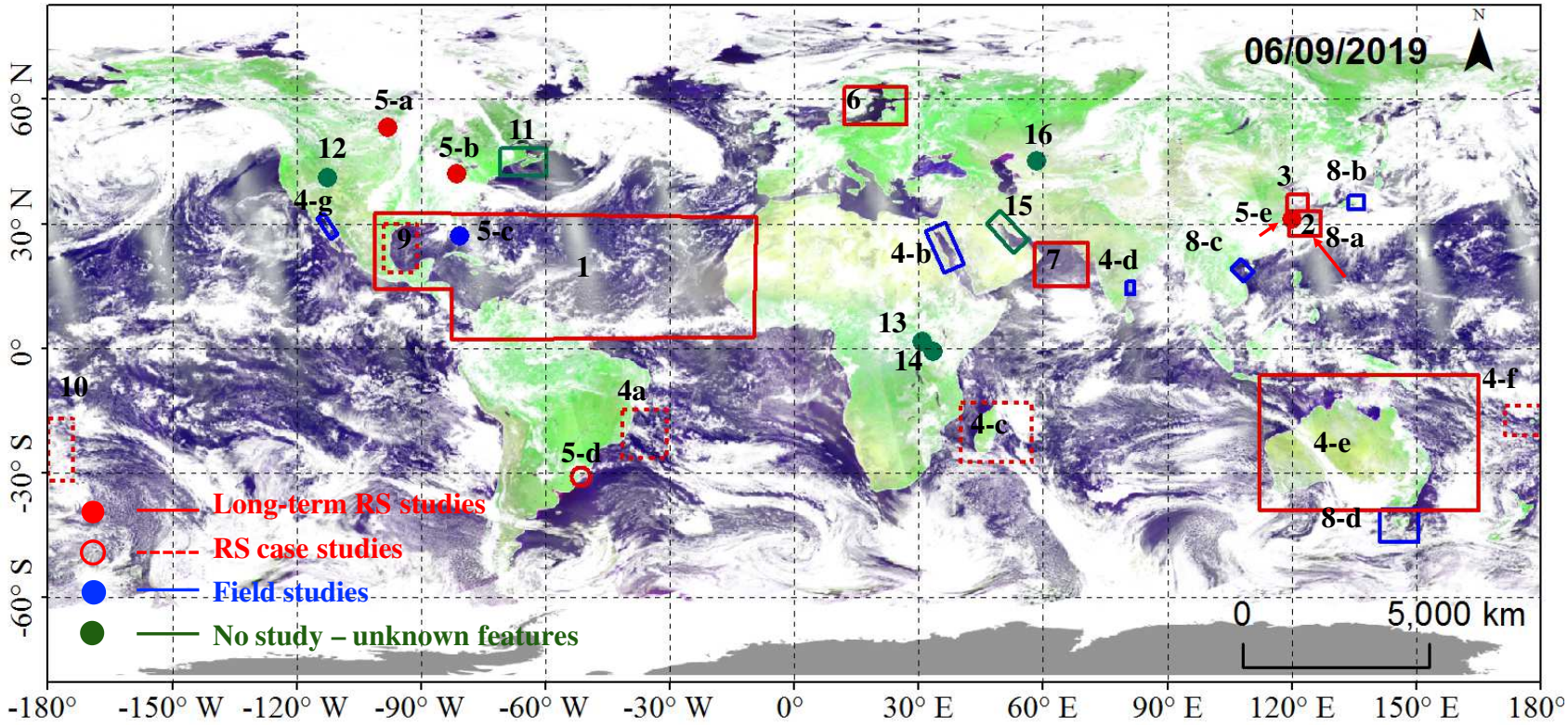

Fig 1. Distribution of floating algae and floating organisms/materials around the world, obtained from inspections of VIIRS FRGB images available through NOAA OCView. The known and unknown features are color coded, with more details provided in Table 2.

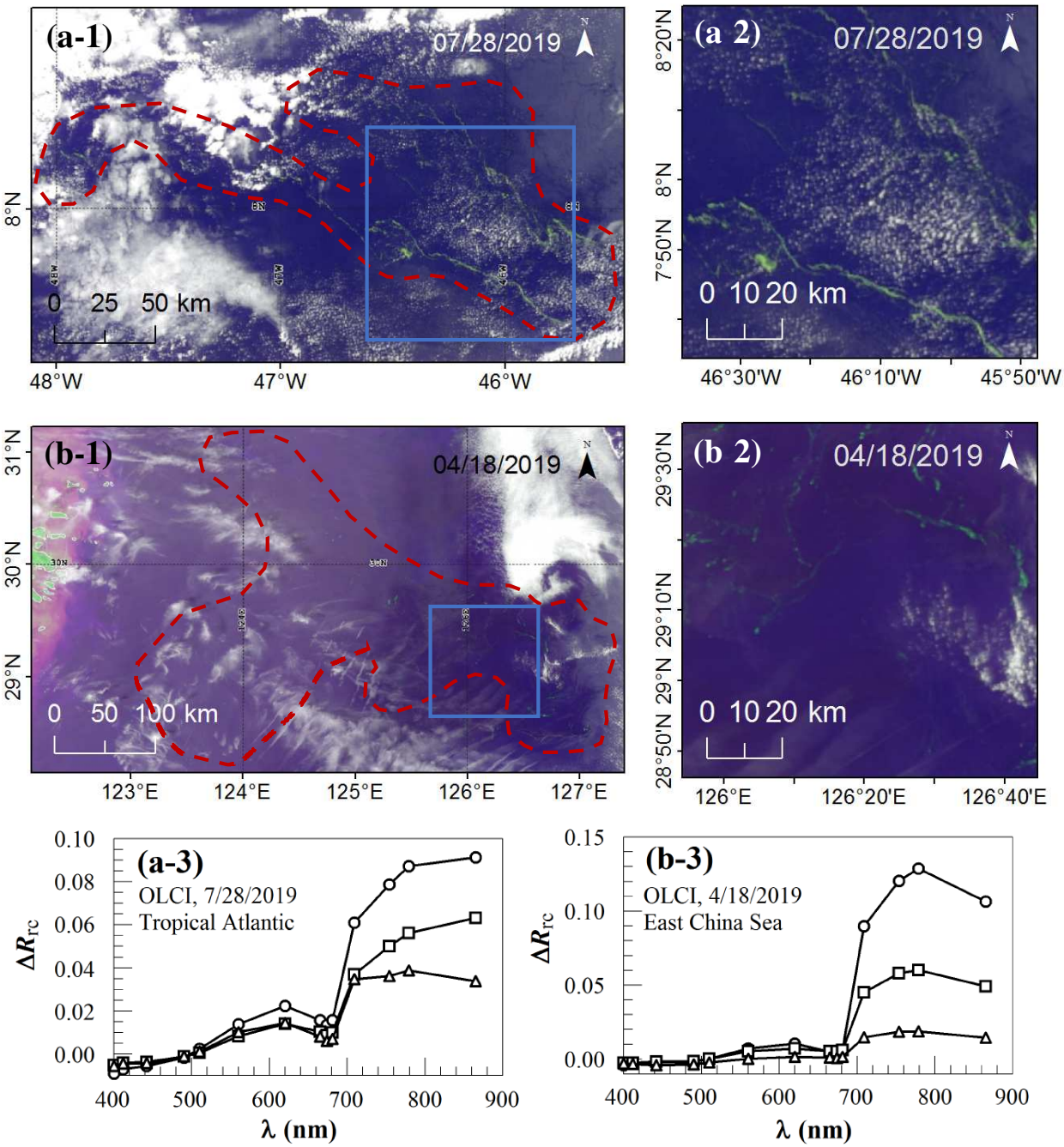

Fig. 2. VIIRS FRGB images show (a) *Sargassum fluitans/natans* in tropical Atlantic (Box 1 in Fig. 1 & Table 2) and (b) *Sargassum horneri* in the East China Sea (Box 2 in Fig. 1 & Table 2). From 6 July to 15 August 2019, similar greenish image slicks can be found in all cloud-free and glint-free FRGB images over the same region in (a). The spectra on the bottom represent typical algae spectra extracted from the corresponding OLCI image pixels.

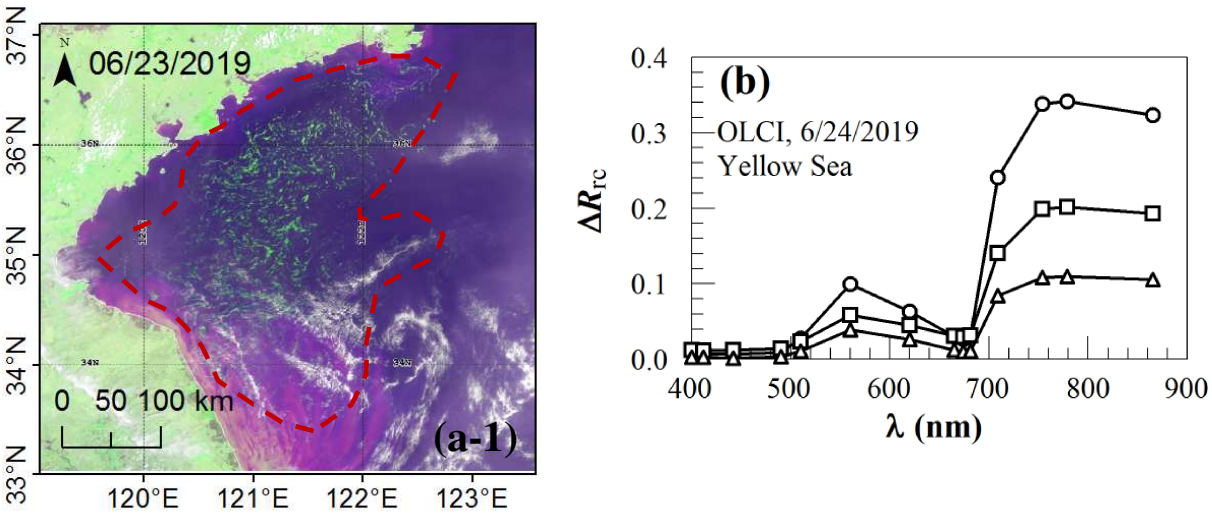

Fig. 3. (a) VIIRS FRGB image shows an *Ulva* bloom in the western Yellow Sea (Box 3 in Fig. 1 & Table 2). (b) Typical OLCI $\Delta R_{rc}(\lambda)$ of several pixels selected from the greenish image features.

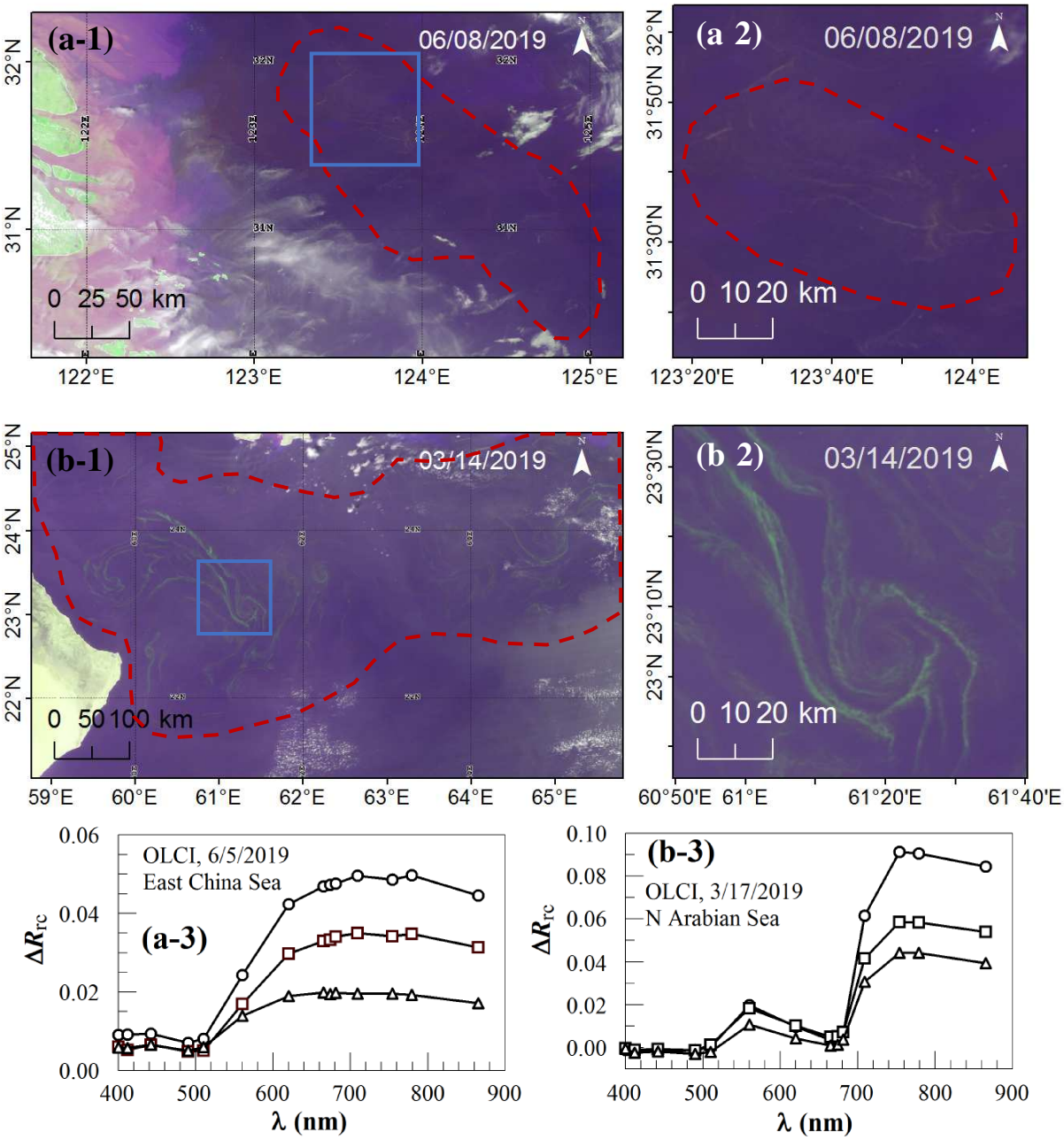

Fig. 4. VIIRS FRGB images show surface aggregations of (a) Red *Noctiluca* in the East China Sea (Box 8a in Fig. 1 & Table 2), (b) Green *Noctiluca* in the northern Arabian Sea (Box 7 in Fig. 1 & Table 2). The areal extents of algae slicks are outlined in red, and the image features from the small squares are enlarged to the right. The OLCI $\Delta R_{rc}(\lambda)$ from the slick features are shown in the corresponding figures in (a-3) and (b-3). More examples of both types of *Noctiluca* can be found in Table 2.

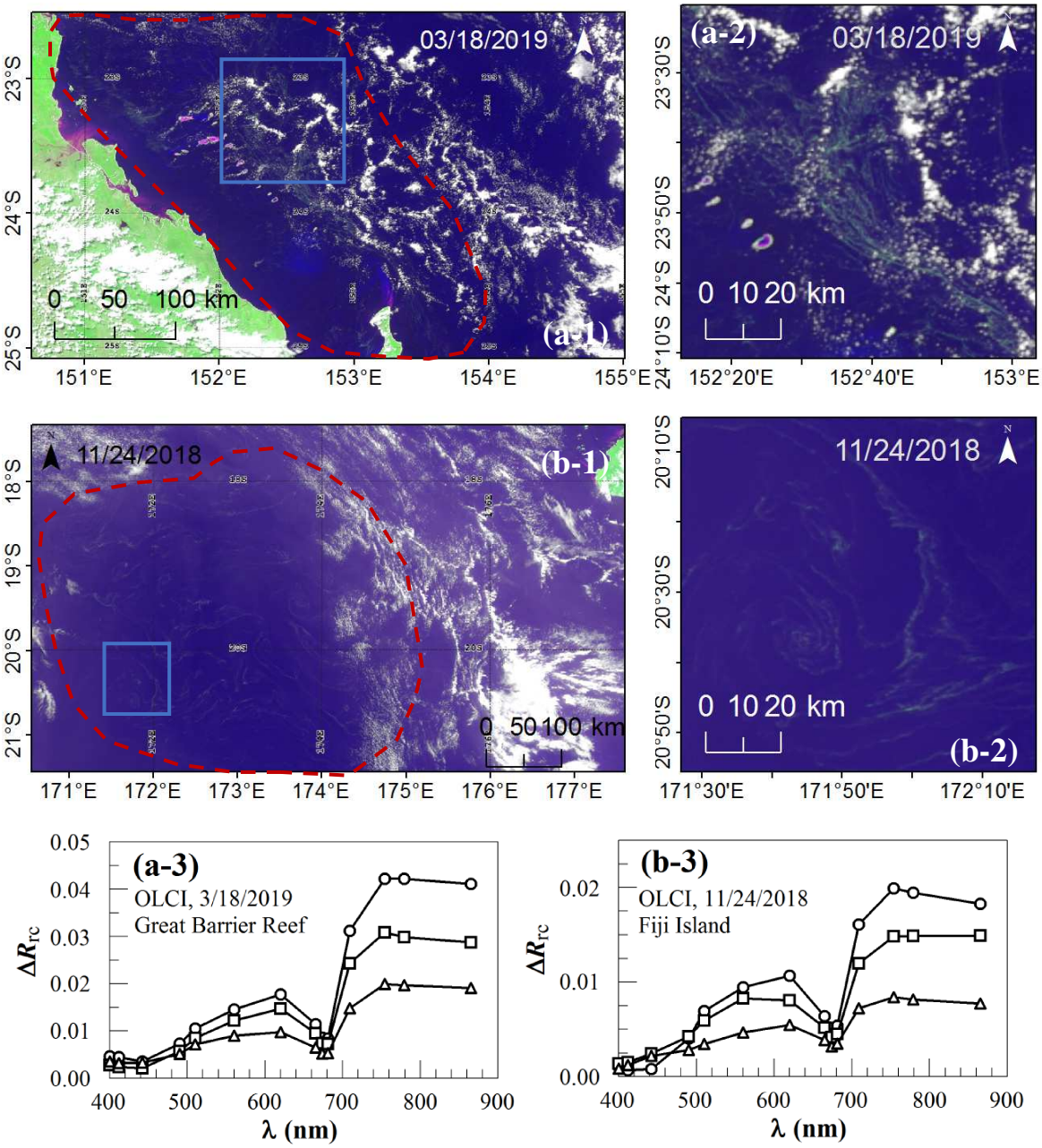
03/18/2019
(a-1)
0 50 100 km
23°S
24°S
25°S
151°E
152°E
153°E
154°E
155°E
(a-2)
03/18/2019
0 10 20 km
23°30'S
23°50'S
24°10'S
152°20'E
152°40'E
153°E
11/24/2018
(b-1)
0 50 100 km
18°S
19°S
20°S
21°S
171°E
172°E
173°E
174°E
175°E
176°E
177°E
11/24/2018
0 10 20 km
(b-2)
20°10'S
20°30'S
20°50'S
171°30'E
171°50'E
172°10'E
(a-3)
OLCI, 3/18/2019
Great Barrier Reef
ΔRrc
λ (nm)
(b-3)
OLCI, 11/24/2018
Fiji Island
ΔRrc
λ (nm)

1056
1057

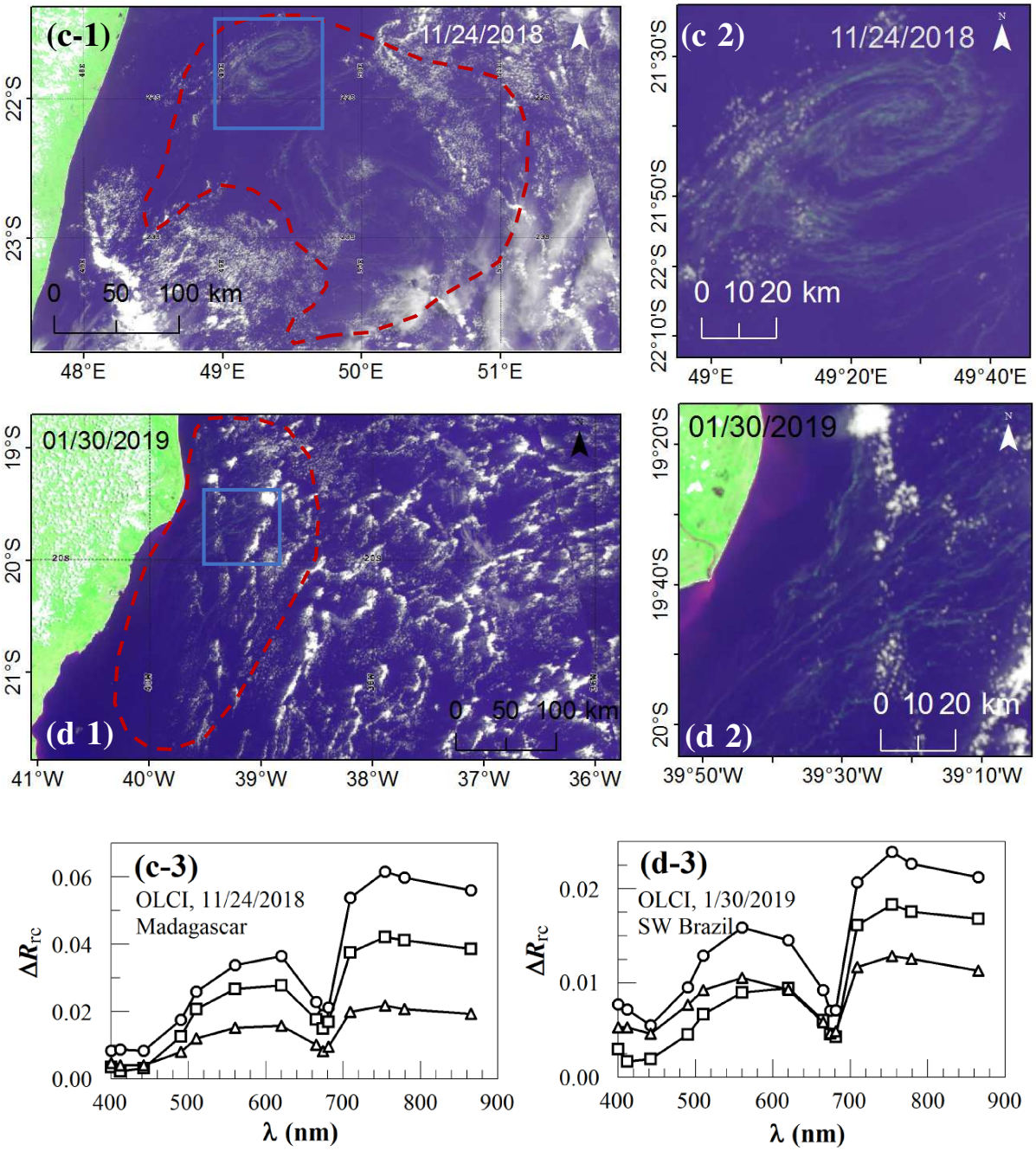

Fig. 5 VIIRS FRGB images show *Trichodesmium* blooms (a-1) around Great Barrier Reef off east coast of Australia, (b-1) around Fiji island in the South Pacific, (c-1) near Madagascar, and (d-1) in the South Atlantic Ocean east of the southwest Brazil. The areal extents of algae slicks are outlined in red, and the image features from the small squares are enlarged to the right. The OLCI-derived $\Delta R_{rc}(\lambda)$ from the slick features are shown in the corresponding figures in (a-3) to (d-3). These features correspond to Boxes 4e, 4f, 4c, and 4a in Fig. 1 & Table 2.

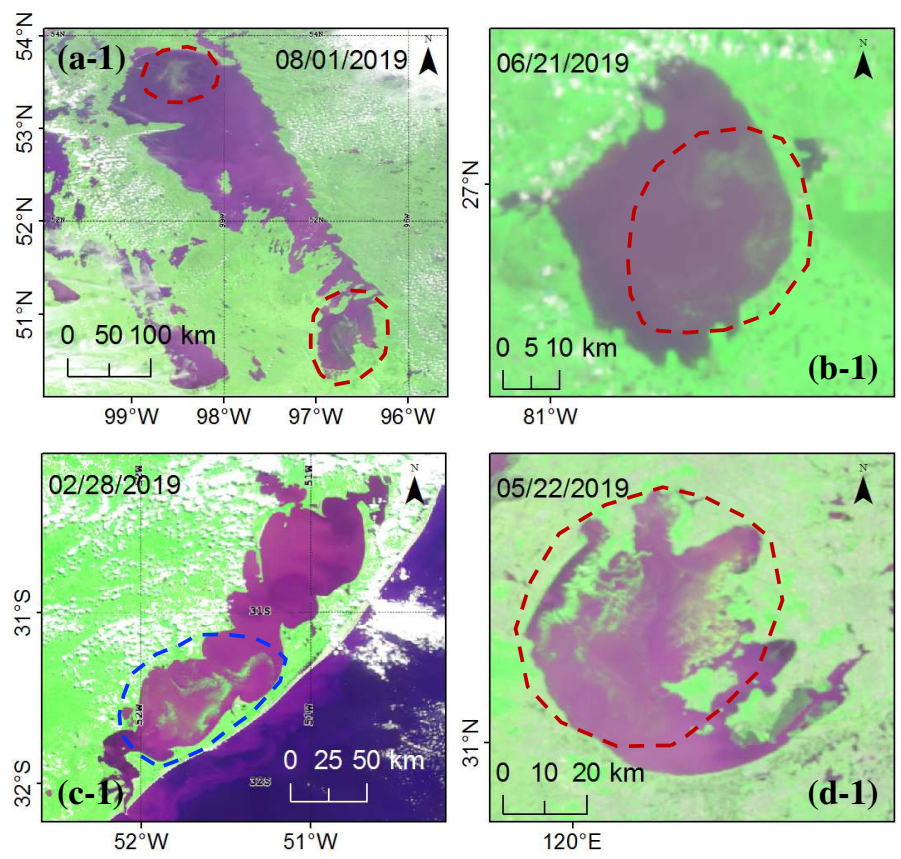

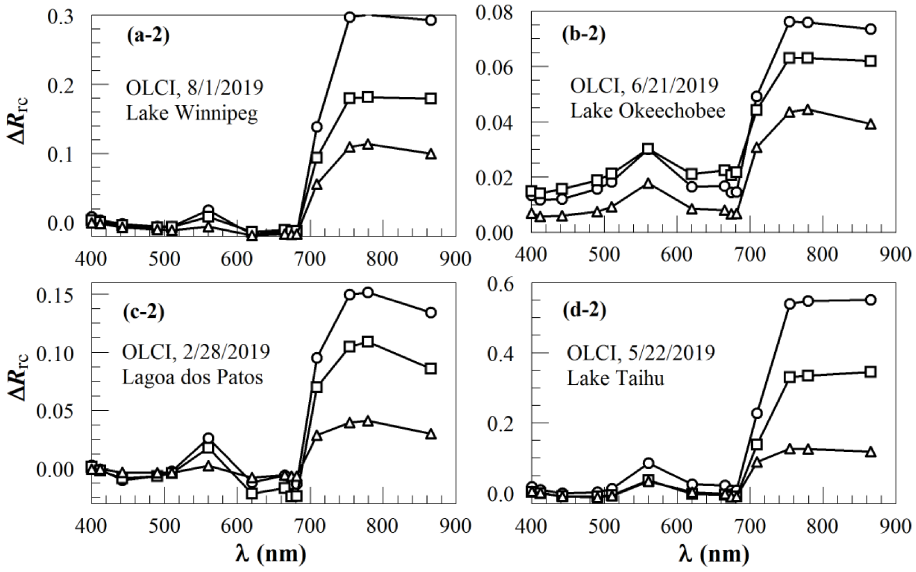

Fig. 6. VIIRS FRGB images show *Microcystis* blooms in (a-1) Lake Winnipeg (Canada), (b-1) Lake Okeechobee (US), (c-1) Lagoa dos Patos (Brazil), and (d-1) Lake Taihu (China). The features are outlined in red, and their corresponding OLCI spectra are shown in (a-2) – (d-2), respectively. These features correspond to Boxes 5a, 5c, 5d, and 5e in Fig. 1 & Table 2, respectively.

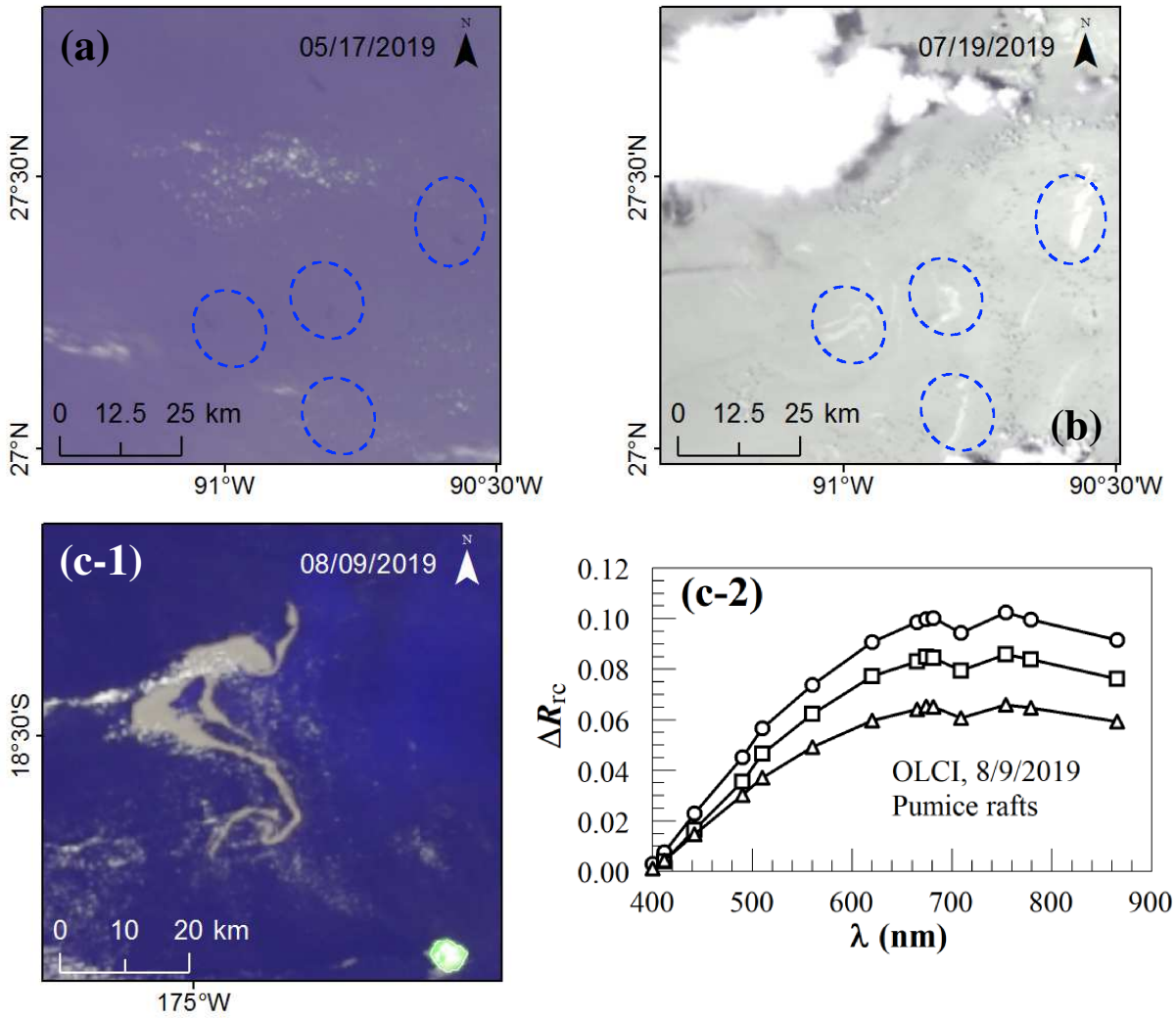

Fig. 7. (a) and (b) VIIRS FRGB images show surface oil slicks due to natural seepage in the NW Gulf of Mexico (Box 9 in Fig. 1 & Table 2). These slicks show dark contrast in (a) and bright contrast in (b) due to different sun glint strengths (Hu et al., 2009). The outlined features can be visualized more clearly after color stretches, but for illustration purpose the original color stretch of the VIIRS FRGB images is kept here. (c-1) VIIRS FRGB image shows pumice rafts on the surface, where the $\Delta R_{rc}(\lambda)$ spectra from several pixels of the same-day OLCI image are shown in (c-2).

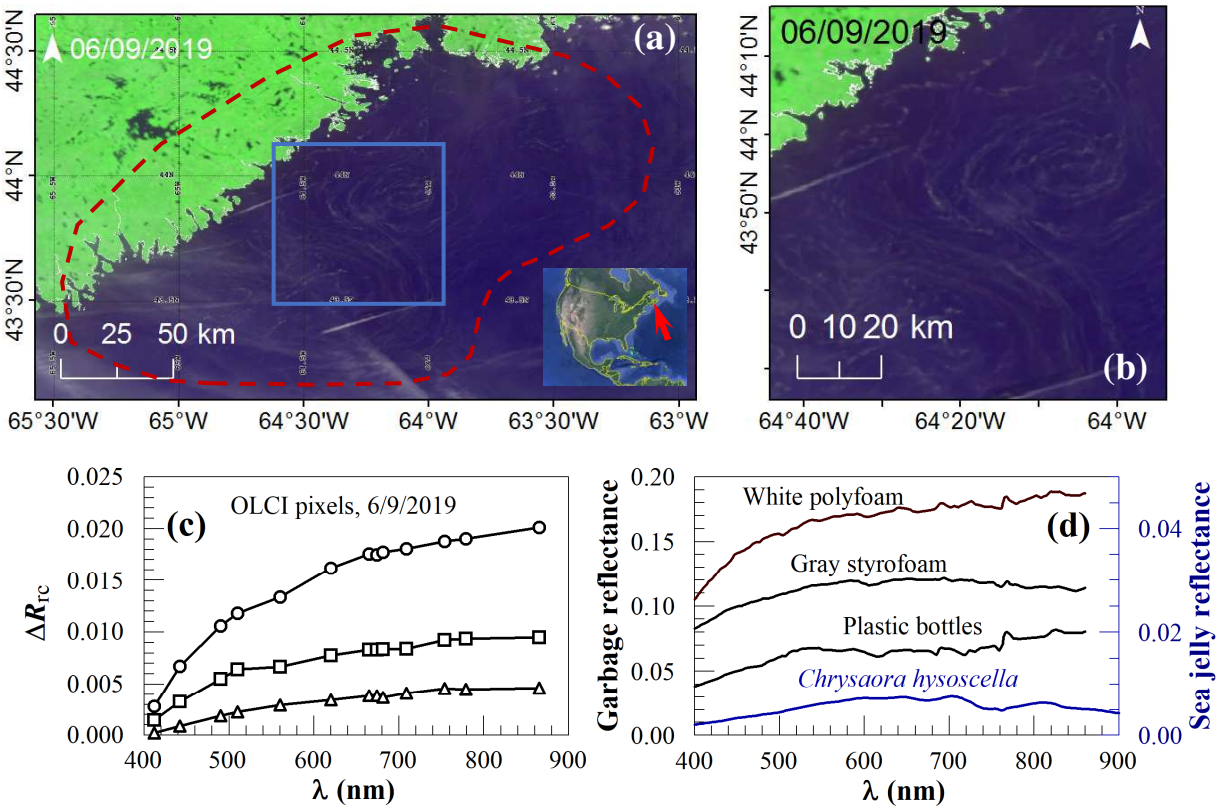

Fig. 8. (a) Surface slicks in VIIRS FRGB image on 9 June 2019 (Box 11 in Fig. 1 & Table 2), from coastal waters off SW Nova Scotia (red arrow in the inset map). (b) A zoom-in image from the rectangular box in (a), where the slicks features can be clearly visualized. (c) ΔR_{rc} spectra of several OLCI pixels from the same slicks in (b); (d) Reflectance spectra of transparent plastic bottles, gray Styrofoam, white polyfoam, and one type of sea jellies (*Chrysaora hysoscella*) (right y-axis). The latter was measured in a lab setting rather than in the ocean environment (Van der Zande et al., 2014).

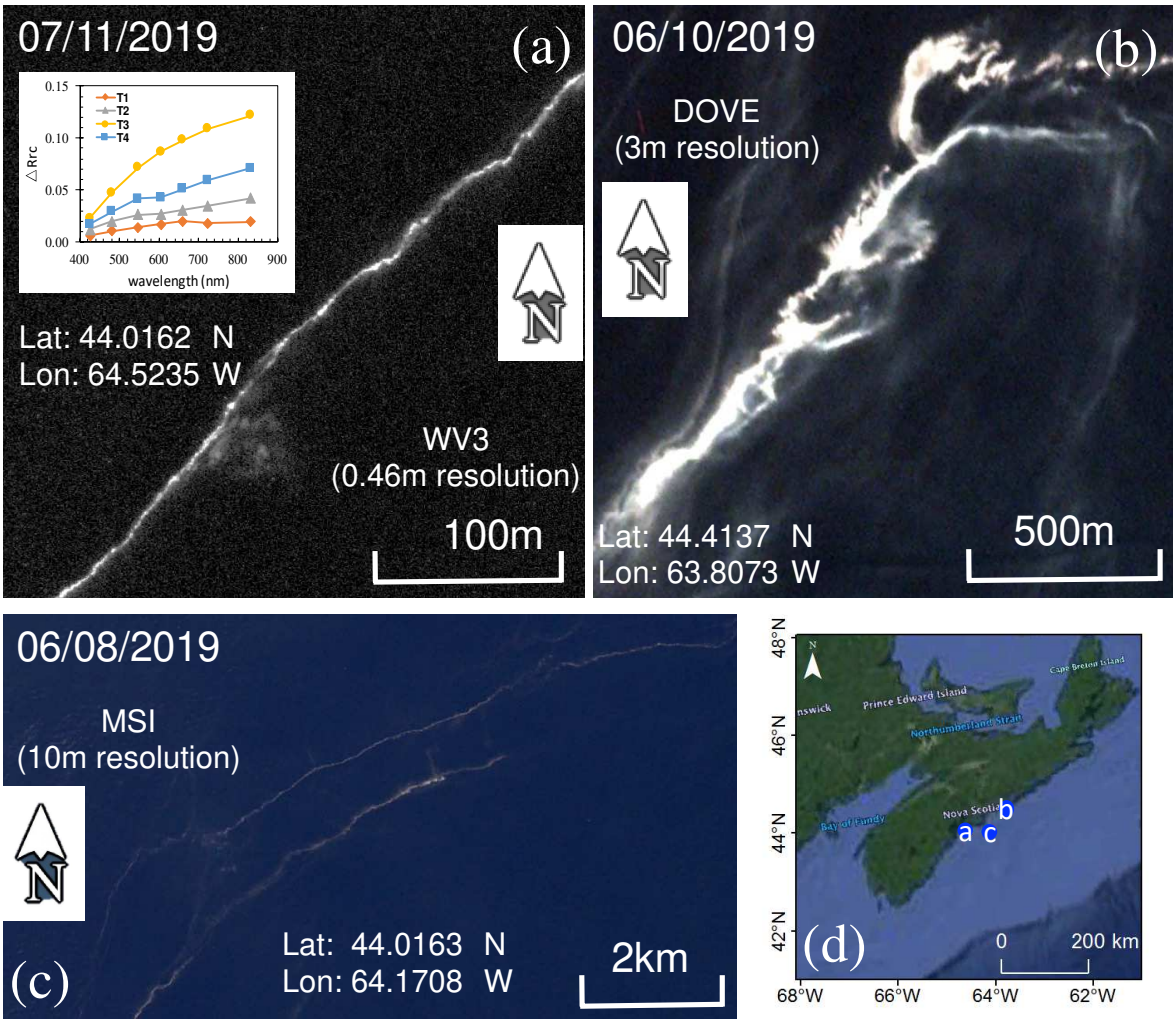

Fig. 9. Surface slicks in (a) WV3 panchromatic-band image on 11 July 2019, (b) DOVE image on 10 June 2019, and (c) MSI image on 8 June 2019 off SW Nova Scotia. These bright image features correspond to some of the features in the VIIRS FRGB image in Fig. 8a. The locations of these images are annotated in (d). The inset figure in (a) shows the ΔR_{rc} spectra of several WV3 pixels from the bright slicks.

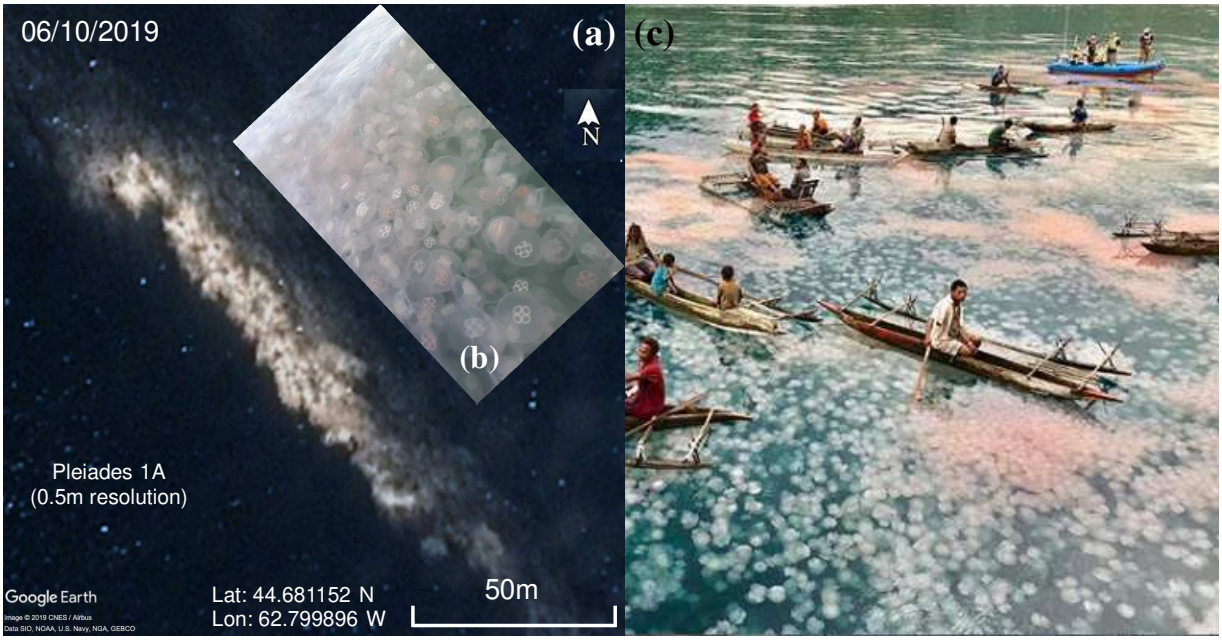

Fig. 10. (a) Pleiades (CNES, image provided by Google Earth) image on 10 June 2019 off SW Nova Scotia showing the bright image features corresponding to some of the features in the VIIRS FRGB image in Fig. 8. (b) Screenshot of a facebook video posted by Leslie Carter on 31 July 2019 in The Gulf Fishing News (https://www.facebook.com/gulfareafishingnews/), which shows a jellyfish bloom north of Nova Scotia. (c) Jellyfish bloom in Milne Bay Province, Papua New Guinea (New Zealand). Image posted online on 10 June 2019 (https://www.facebook.com/discoverpng/).

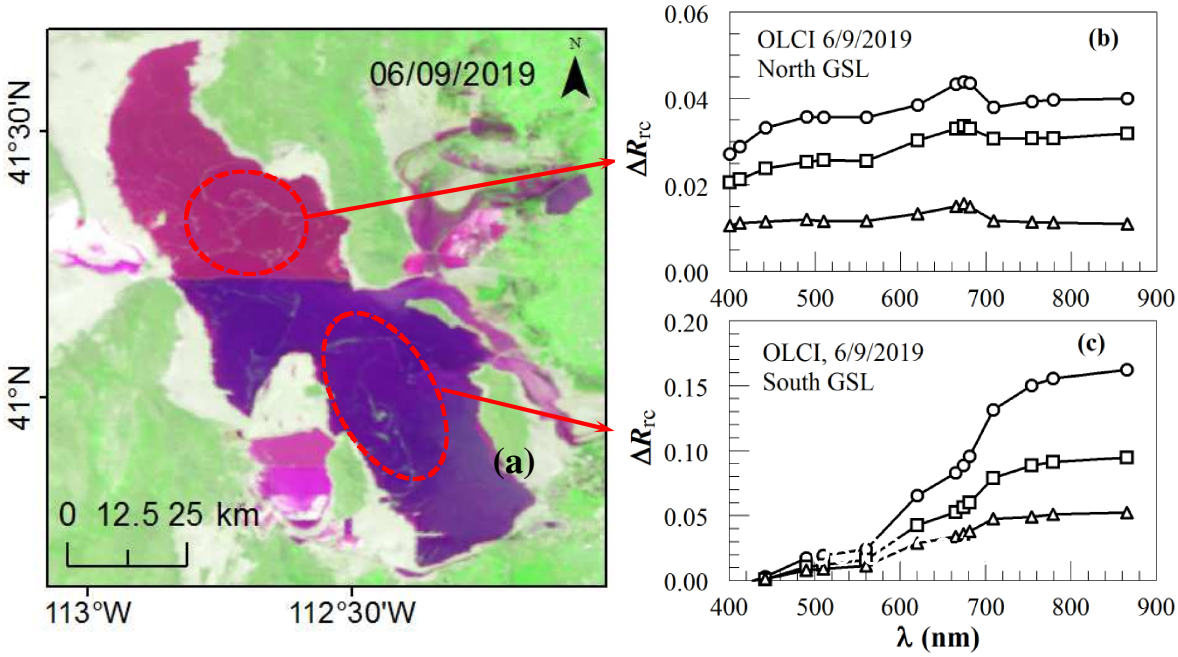

Fig. 11. (a) VIIRS FRGB image over the Great Salt Lake (Utah, US, Box/dot 12 in Fig. 1 & Table 2) showing slicks in both the north arm and south arm of the lake, separated by a west-east railroad causeway. (b) – (c) ΔR_{rc} spectra of several OLCI pixels from these slick features, indicating 1) unknown features in (b), and 2) possibly floating brine shrimp cysts (resting eggs) in (c).

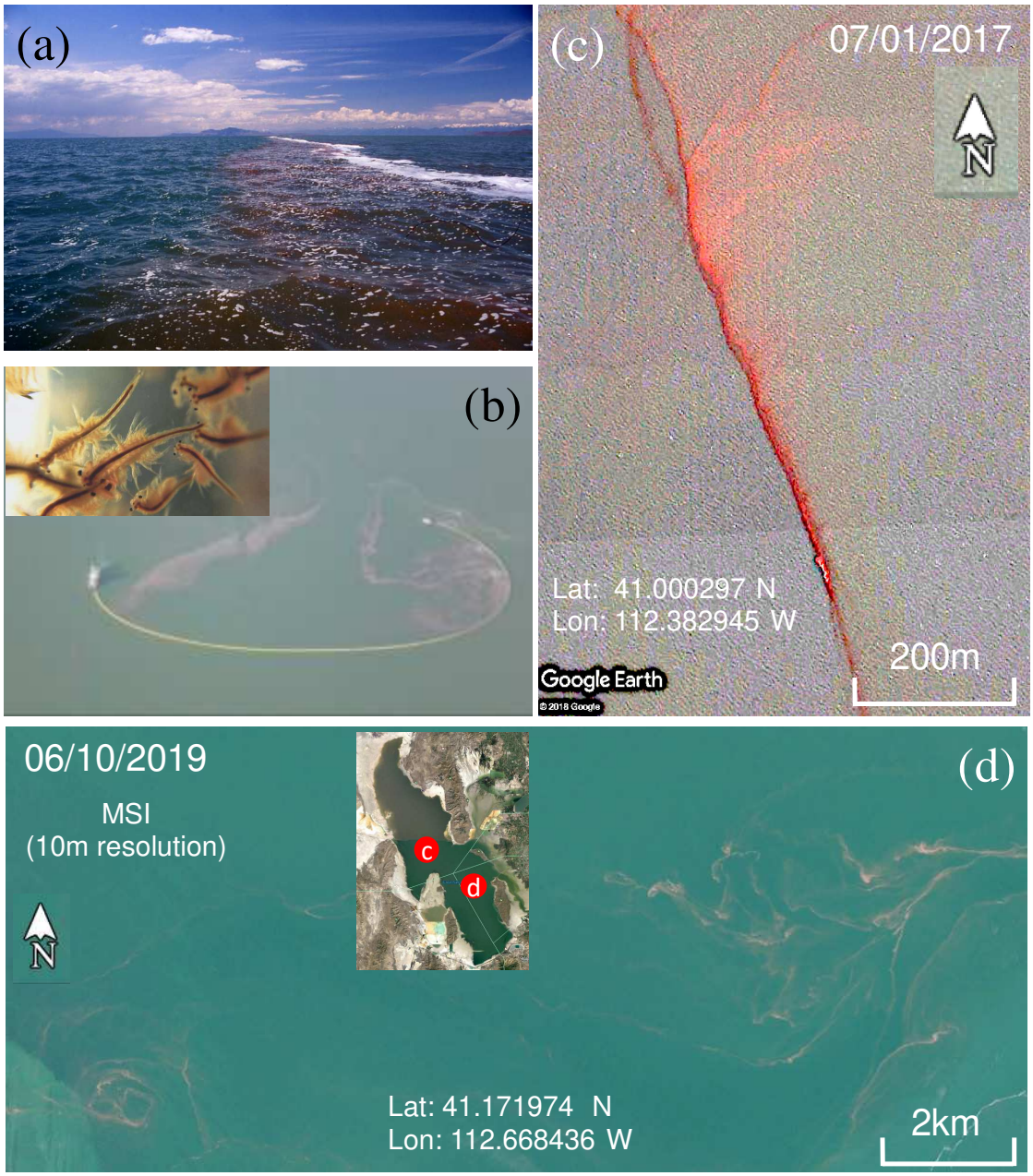

Fig. 12. (a) Surface aggregation of brine shrimp (*Artemia*) eggs in the Great Salt Lake (photo taken by Gilbert Bay on 24 June 2009); (b) An airborne photo shows corralling of brine shrimp eggs for harvesting (photo courtesy of https://saltlakebrineshrimp.com/harvest/). The inset figure shows the brine shrimp, with an average length of ~0.7 – 1.3 cm for adults. (c) Google Earth image on 1 July 2017 shows surface aggregation of brine shrimp eggs in the Great Salt Lake. (d) MSI true-color RGB image on 10 June 2019 shows image slicks where the spectral shapes appear to be similar to those of Fig. 11b, therefore possibly caused by aggregations of brine shrimp eggs. The insert map shows the locations of (c) & (d) in the Great Salt Lake.

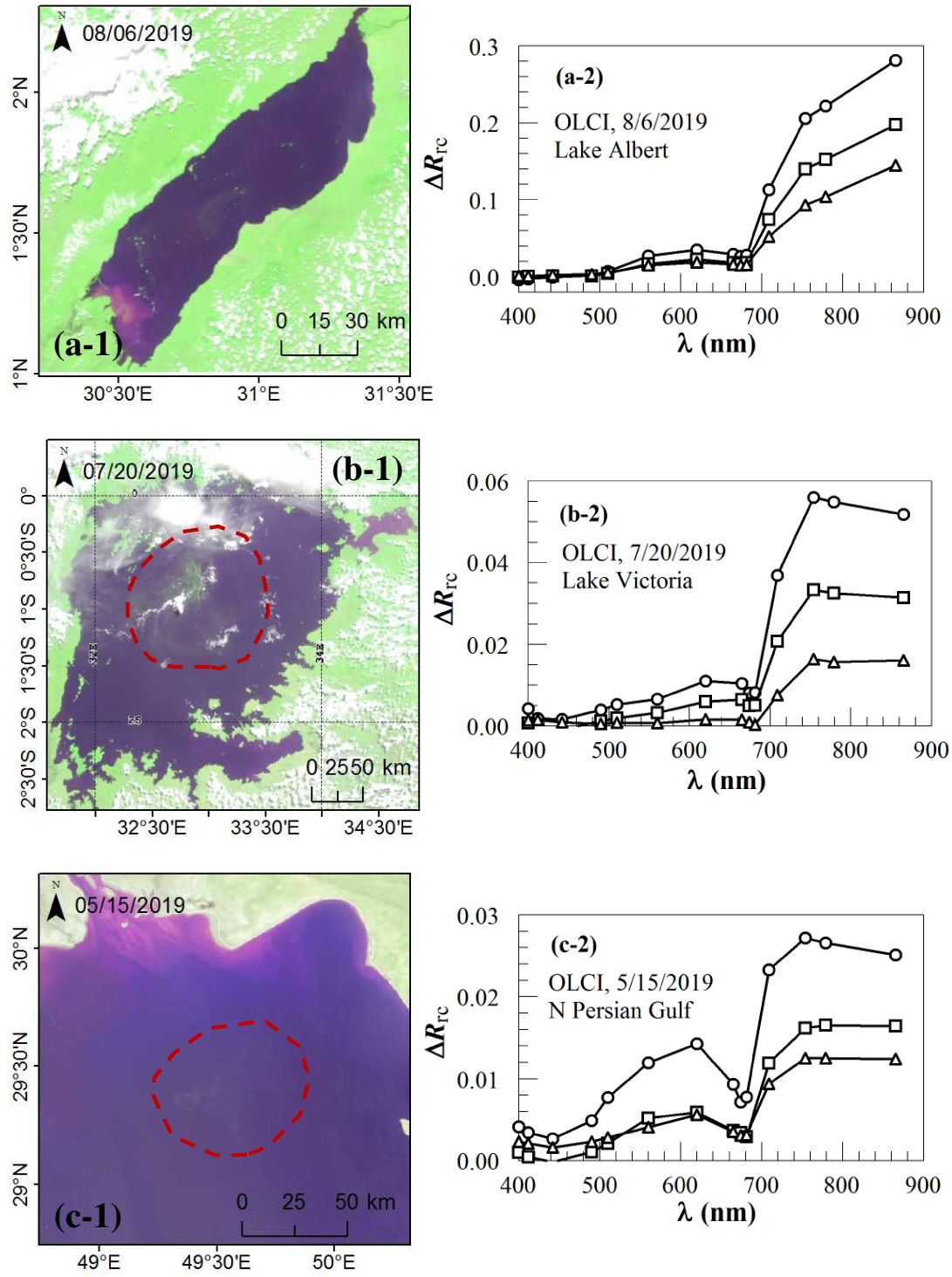

Fig. 13. VIIRS FRGB images show surface algae slicks in (a-1) Lake Albert (on the border of Uganda and Congo of Africa, Box/dot 13 in Fig. 1 & Table 2); (b-1) Lake Victoria (between Uganda Tanzania and Kenya of Africa, Box/dot 14 in Fig. 1 & Table 2); (c-1) northern Persian

(Arabian) Gulf (Box/dot 15 in Fig. 1 & Table2). The OLCI $\Delta R_{rc}(\lambda)$from the slick features are shown in the corresponding figures in (a-2) – (c-2), respectively.